รายงานวิจัยฉบับสมบูรณ์

โครงการ แบบจำลองคณิตศาสตร์สำหรับการแยกชีวโมเลกุลโดยใช้ท่อขนาดนาโนเมตร
(Modelling a purification of biomolecules utilizing nanoporous material)

ผศ.ดร.ดวงกมล เบ้าวัน

มิถุนายน 2558

สัญญาเลขที่ TRG5680072

รายงานวิจัยฉบับสมบูรณ์

โครงการ แบบจำลองคณิตศาสตร์สำหรับการแยกชีวโมเลกุลโดยใช้ท่อขนาดนาโนเมตร
(Modelling a purification of biomolecules utilizing nanoporous material)

ผศ.ดร. ดวงกมล เบ้าวัน (หัวหน้าโครงการ)
ภาควิชาคณิตศาสตร์ คณะวิทยาศาสตร์ มหาวิทยาลัยมหิดล

รศ.ดร. งามตา ธรรมวัฒนะ (นักวิจัยที่ปรึกษา)
Faculty of Engineering and Information Sciences, University of Wollongong

สนับสนุนโดยสำนักงานกองทุนสนับสนุนการวิจัยและมหาวิทยาลัยมหิดล

(ความเห็นในรายงานนี้เป็นของผู้วิจัย สกว. และมหาวิทยาลัยมหิดลไม่จำเป็นต้องเห็นด้วยเสมอไป)

Abstract

The selective separation and purification of biological molecule is importance in the food and pharmaceutical industries. This project aims to determine the adsorption energy of proteins onto/in nano-materials. The relation between a biomolecule size and a nanoporous radius is examined to optimize the adsorption energy. Once we obtain a pure or a selective biological molecule(s), the loading of such molecule on other type of nanoparticles is determined as a first step to design a cargo in drug delivery system. An energy behaivour for the interaction between protein and nanoparticle is studied. On utilizing a continuous approximation, the electrostatic and van der Waals interactions can be analytically expressed using the integral technique. The Columbic function is employed as a force field for the electrostatic energy and the 6-12 Lennard-Jones function is utilized to determine the van der Waals interaction. This mathematical model can help a trial and error process in an experiment and might be viewed as a first to design a drug molecule in a pharmaceutical industry.

Keywords: Biomolecules, Continuum approximation, Interaction energy, Mathematical model

บทคัดย่อ

การคัดเลือกและการทำให้โมเลกุลทางชีวภาพบริสุทธิ์เป็นเรื่องที่สำคัญในอุตสาหกรรมอาหารและยา โครงการนี้มีวัตถุประสงค์เพื่อศึกษาการดูดซับโปรตีนบนวัสดุที่มีขนาดนาโนเมตร โดยพิจารณาความสัมพันธ์ระหว่างพลังงานของระบบ ขนาดของโปรตีน และรัศมีของท่อนาโนเมตรที่ใช้ในการคัดแยกสาร เมื่อเราได้โมเลกุลทางชีวภาพที่คัดแยกออกมาแล้ว เราจะพิจารณาการบรรจุโมเลกุลดังกล่าวลงในแคปซูลขนาดจิ๋วและพิจารณาการเคลื่อนที่ของโมเลกุลผ่านเยื่อไขมัน ซึ่งเป็นขั้นตอนแรกในการออกแบบระบบการจัดส่งยา ในที่นี้พลังงานสำหรับการปฏิสัมพันธ์ระหว่างโปรตีนและอนุภาคนาโนที่ใช้คือพลังงานไฟฟ้าสถติ (Electrostatic) ที่เกิดจากฟังก์ชันคูลอมบ์ (Columbic potential) และแรงระหว่างโมเลกุล (Van der Waal) ที่เกิดจากฟังก์ชันเลนาท-โจนท์ (Lennard-Jones potential) และใช้สมมติฐานของความต่อเนื่องในการหาพลังงานรวมของระบบ ซึ่งแบบจำลองทางคณิตศาสตร์ที่ได้จากงานวิจัยชิ้นนี้สามารถช่วยลดขั้นตอนการสุ่มทดลองในห้องปฏิบัติการ และอาจถือได้ว่าแบบจำลองนี้เป็นพื้นฐานในการออกแบบระบบการส่งโมเลกุลยาเข้าสู่ร่างกายสำหรับอุตสาหกรรมยาได้อีกด้วย

Executive Summary

1. ความสำคัญและที่มาของปัญหา

Detecting single molecule is an enabling capability for fundamental science in fields such as biophysics and chemistry and a useful advancement for applied fields such as medicine, environmental pollution monitoring and defense. Developing sensors that are capable of detecting individual molecules has therefore become an important field of research. Biological pores stand out as relatively simple components of single-molecule sensors. In nature, a large number of cellular functions such as cell adhesion, cell signaling, or the action of therapeutic drugs depend on molecular binding interactions such as ligand-receptor interactions. Understanding these interactions is therefore important both for fundamental science and for the design of therapeutically effective modulators.

This project will study the binding mechanisms between biomolecules and nanopores. The change in the structural and total interaction energy of such a system will give rise to a molecular force which can be measured for sensing purposes. The significance of this project is that it will provide a basic understanding and an accurate predictive capacity for a number of complex biological and medical processes involved in the binding mechanisms of nanoparticles and biological pores. Detailed and accurate modelling will accelerate the development of targeted drug delivery applications.

2. วัตถุประสงค์

1. Model the interaction energy between biomolecules and nanopores to determine the suction energy arising from the pores to encapsulate the foreign molecule. A main result from the model will be an energy function in terms of biomolecule sizes and nanopore radii.
2. Determine the number of biomolecules coating a nanoparticle.
3. Analyse the mathematical model in terms of a numerical result and compare our results with previous computational or experimental works.
4. Use computer simulation technique to confirm mathematical finding.

3. ระเบียบวิธีวิจัย

1. Formulate a mathematical model to determine an interaction energy between biomolecule and nanoporous where Lennard-Jones potential and the continuous approximation are utilized.
2. In the case that there exists an electrostatic energy in the system, the Columbic potential may be included.
3. Find an analytical expression to determine a molecular interaction between a biomolecule (protein) and nanopores.
4. Use computer simulation technique such as molecular dynamic simulation or molecular mechanic simulation to compare the result with the one obtained by mathematical model.
5. Examine our mathematical model(s) numerically and compare our results with others.
6. Modify our model to incorporate environment factors for example temperature and pressure of the system to make our model be more realistic.

4. แผนการดำเนินงานวิจัยตลอดโครงการในแต่ละช่วง 6 เดือน

First year

Activities	Months 1-3	Months 4-6	Months 7-9	Months 10-12
1. Study the literature review to finalise our research aim.	← →			
2. Formulate mathematical model to explain the interaction energy between biomolecules and nanopores.	←	← →		
3. Determine our model numerically.		←	← →	
4. Analyse our results and compare with computational simulation method.			←	→
5. Write a manuscript and submit for publication.			←	→

Second year

Activities	Months 1-3	Months 4-6	Months 7-9	Months 10-12
1. Formulate mathematical model to determine a number of protein molecules surrounding a nanoparticle	←	→		
2. Modify our model to include environmental effects, i.e. temperature and pressure.	←	→		
3. Determine our model numerically.		←	→	
4. Analyse our results and compare with computational simulation method.		←	→	
5. Write a manuscript and submit for publication.			←	→
6. Attend a conference.	←	→	→	→

5. ผลงาน/หัวข้อเรื่องที่คาดว่าจะตีพิมพ์ในวารสารวิชาการระดับนานาชาติ

ชื่อเรื่องที่คาดว่าจะตีพิมพ์ : Mathematical model for a spherical nanoparticle encapsulated in a lipid nanotube

ชื่อวารสารที่คาดว่าจะตีพิมพ์ : Journal of Mathematical Chemistry

ค่า impact factor : 1.303

ชื่อเรื่องที่คาดว่าจะตีพิมพ์ : Energy behaviour for serum albumin inside nanopores

ชื่อวารสารที่คาดว่าจะตีพิมพ์ : Microporous and Mesoporous Materials

ค่า impact factor : 3.285

6. งบประมาณโครงการ (ตามระยะเวลาโครงการที่ได้เสนอรับทุน โดยงบประมาณไม่เกิน 240,000 บาท/ปี)

	ปีที่ 1	ปีที่ 2	รวม
1. หมวดค่าตอบแทน - ค่าตอบแทนหัวหน้าโครงการ 10,000 x 12 / ปี	**120,000**	**120,000**	**240,000**
2. หมวดค่าวัสดุ - ค่าวัสดุทั่วไป อาทิเช่น วัสดุสำนักงาน - ค่าอุปกรณ์อัพเกรดคอมพิวเตอร์ อาทิเช่น ฮาร์ดดิสก์ และ แรม	**10,000** 7,500 2,500	**10,000** 7,500 2,500	**20,000**
3. หมวดค่าใช้สอย - ค่าถ่ายเอกสาร - ค่าตีพิมพ์ผลงานวิชาการ - ค่าเข้าร่วมประชุมวิชาการ - ค่าเดินทางเพื่อทำวิจัยและนำเสนอผลงาน	**15,000** 5,000 10,000 - -	**40,000** 5,000 10,000 10,000 15,000	**55,000**
4. ครุภัณฑ์ - Computer notebook [1]	**60,000** 60,000	-	**60,000**
รวมงบประมาณโครงการ	**205,000**	**170,000**	**375,000**

หมายเหตุ: เครื่องหมาย - หมายถึง ให้ใส่รายละเอียดรายการใช้จ่ายในแต่ละหมวด

[1] งานวิจัยหลักของโครงการวิจัยนี้คือการคำนวณโดยใช้คอมพิวเตอร์ จึงจำเป็นที่ต้องใช้เครื่องคอมพิวเตอร์ที่มีคุณภาพดีในการคำนวณ ดังนั้นจึงมีความจำเป็นที่ต้องซื้อเครื่องคอมพิวเตอร์โน้ตบุคสำหรับงานวิจัยนี้

รายละเอียดโครงการ

ชื่อโครงการ: แบบจำลองคณิตศาสตร์สำหรับการแยกชีวโมเลกุลโดยใช้ท่อขนาดนาโนเมตร
Modelling a purification of biomolecules utilizing nanoporous material

ชื่อหัวหน้าโครงการ

(ภาษาไทย): นางสาว ดวงกมล เบ้าวัน

(ภาษาอังกฤษ): Miss Duangkamon Baowan

(ตำแหน่งวิชาการ): ผู้ช่วยศาสตราจารย์

ระยะเวลาดำเนินงาน : 2 **ปี** - **เดือน**

เวลาทำงานวิจัยในโครงการประมาณสัปดาห์ละ 17.5 **ชั่วโมง**

สถานที่ติดต่อ :

ที่ทำงาน ภาควิชาคณิตศาสตร์ คณะวิทยาศาสตร์ มหาวิทยาลัยมหิดล

โทรศัพท์ 022015350, 0850760800

โทรสาร 022015434

e-mail duangkamon.bao@mahidol.ac.th

ชื่อนักวิจัยที่ปรึกษา

(ภาษาไทย): นางสาวงามตา ธรรมวัฒนา

(ภาษาอังกฤษ): Miss Ngamta Thamwattana

(ตำแหน่งวิชาการ): Associate Professor

สถานที่ติดต่อ :

ที่ทำงาน School of Mathematics and Applied Statistic,
University of Wollongong,
Wollongong NSW 2522 AUSTRALIA

โทรศัพท์ +61 2 42214630

โทรสาร +61 2 42214845

e-mail ngamta@uow.edu.au

เนื้อหางานวิจัย

Here we focus on using applied mathematical model to determine the energy for the systems consisting of bionanomolecules. Lennard-Jones potential function is utilized as a force field, and the continuous approximation where atoms on a molecule is assumed to be uniformly distribution on the surface or the volume of the molecule is employed to determined the total energy of the system.

Continuous Lennard-Jones approach

For much of this research we are concerned with evaluating the van der Waals interaction energy between atoms, molecules and nanostructures. There are a number of different potential functions which may be used to model the van der Waals potential function. However, we will primarily concern ourselves with the Lennard-Jones potential function $\Phi(\rho)$ which for two non-bonded atoms may be written in the form

$$\Phi(\rho) = -\frac{A}{\rho^6} + \frac{B}{\rho^{12}} \tag{1}$$

where ρ is the distance between the interacting atoms, and *A* and *B* are empirically determined constants of attraction and repulsion, respectively. The graph of Lennard-Jones potential function is as shown in Fig. 1. When calculating the van der Waals interaction between molecules containing a number of atoms, the pairwise interactions may be summed to derive a total interaction *E* which is given by

$$E = \sum_i \sum_j \Phi(\rho_{ij}) \tag{2}$$

where the indices *i* and *j* vary over all the atoms in each molecule and ρ_{ij} denotes the distance between atoms *i* and *j*. Obviously this formulation requires that we know the precise location of every atom in both molecules and we are required to perform *ij* individual calculations of the potential function $\Phi(\rho_{ij})$ to calculate the total interaction energy for the two molecules. These two considerations can be inconvenient or unnecessarily intensive computationally for situations when the exact orientations of the molecules are not specified or when large nanostructures are involved. Therefore, for most of this book we will make an approximation where we assume that all the atoms are smeared over ideal lines or surfaces which represent the molecules that we are modelling. With this approximation we are able

to replace the explicit summations in (2) with line or surface integrals that allow us to write

$$E = \eta_1 \eta_1 \int_{S_1} \int_{S_2} \Phi(\rho) dS_2 dS_1 \tag{3}$$

where here ρ denotes the distance between typical infinitesimal surface elements dS_1 and dS_2 of the lines or surfaces S_1 and S_2, respectively, and the terms η_1 and η_2 are the atomic densities (i.e. atoms per unit surface area) of the surfaces S_1 and S_2, respectively.

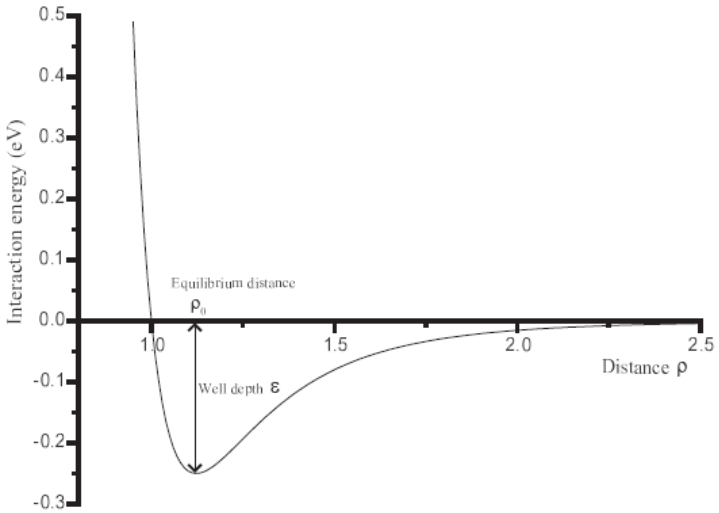

Fig.1 Lennard-Jones function

From these considerations we see that the task of calculating the van der Waals interactions will be made considerably easier provided that there are methods to readily evaluate integrals of the form of (3) over various lines and surfaces which are relevant to problems in nanotechnology. It turns out that many of the molecules and nanostructures that we encounter can be modelled very realistically by the basic geometric objects of points, straight lines, flat planes, spheres and right circular cylinders, and therefore integrals over these objects will be needed frequently throughout the remainder of this research. Accordingly, the purpose of here is to address these integrals in a systematic way to facilitate the evaluation of ideal van der Waals interactions.

When we investigate the form of the Lennard-Jones potential function $\Phi(\rho)$ given in (1) in the context of the integral formulation of (3) we note that the attractive term ρ^{-6} and the repulsive term ρ^{-12} can be separated and integrated independently. We also note that the two terms only vary in terms of the coefficients *A* and *B*, and the magnitude of the index which is applied to the distance variable ρ. In subsequent sections we shall occasionally make use of the fact that the indices of ρ in (1) are both negative even integers which leads us to express the Lennard-Jones potential function $\Phi(\rho)$ in the form

$$\Phi(\rho) = -AI_3(\rho) + BI_6(\rho) \tag{4}$$

where $I_n(\rho) = \rho^{-2n}$ and we will consider evaluating integrals of the form

$$I = \int_{S_1}\int_{S_2} I_n(\rho) dS_2 dS_1 \tag{5}$$

Finally, we must comment on why we seek analytical evaluation to integrals of the form given in (5). While such integrals can be handled reasonably easily using numerical methods it should be remembered that our goal is to elucidate as much as possible from the models that we develop. In some cases, this can involve constructing a broad landscape of data which might be extremely costly or even inaccessible using purely numerical methods but which may be accessed by evaluating analytical expressions for the potential functions in question. Analytical expressions can also be employed to derive expressions for other quantities, like the force experienced by a molecule would otherwise only be determined by further numerical evaluation. One can always move from the analytical to the numerical but the reverse is not possible.

Interaction of spherical objects

❖ Spherical coordinate system

There are, unfortunately, a number of different conventions that authors have adopted in defining a spherical coordinate geometry. Therefore, to avoid confusion and to introduce the reader to spherical coordinates we begin with a

description of the convention that we adopt here which is that most commonly adopted in the scientific literature.

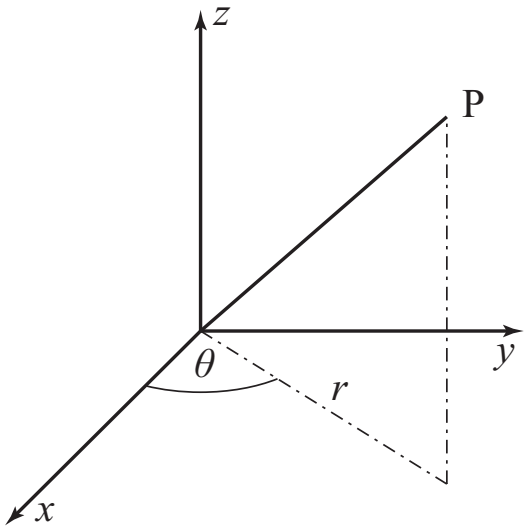

Fig.2 A general point **P** described by spherical coordinates (r,θ,ϕ)

We define a spherical coordinate system (r,θ,ϕ) and define r the radial distance, θ the azimuthal angle, and ϕ the polar angle, as illustrated in Fig. 2. These are oriented with respect to a Cartesian coordinate system (x,y,z) such that θ is measured in the *xy*-plane beginning from the positive *x*-axis and proceeding in an anticlockwise direction. The polar angle ϕ is then measured from the positive direction of the *z*-axis and proceeds down to the negative direction. Therefore, the coordinates have primary values of $r\in[0,\infty)$, $\theta\in(-\pi,\pi]$ and $\phi\in[0,\pi]$.

Next we will be considering various integrals of the Lennard-Jones potential function $\Phi(\rho)$ over the surface of a sphere of radius *a*. In such cases the integral considered will be of the form

$$I = a\int_0^{\pi}\int_{-\pi}^{\pi}\frac{\sin\phi}{\rho^{2n}}d\theta d\phi$$

where ρ is some function of the geometric parameters of the problem, which will generally be a function of θ and ϕ.

❖ Interaction of point with a sphere

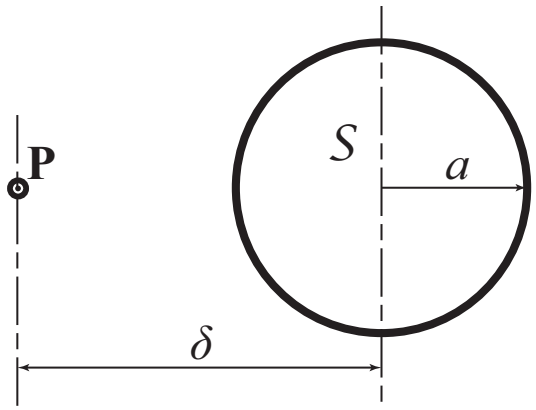

Fig. 3 Sphere $\mathbf{S}$ of radius *a*, interacting with point $\mathbf{P}$ at a distance of δ from centre of the sphere.

We begin by considering a point given in Cartesian coordinates as $\mathbf{P}=(0,0,\delta)$, which is at a distance δ from the centre of a sphere of radius *a* which is parameterised in spherical coordinates as $S(\theta,\phi)=(a,\theta,\phi)$, as illustrated in Fig. 3. In these coordinates the integral of interest (5) is given by

$$I=a^2\int_0^{\pi}\int_{-\pi}^{\pi}\frac{\sin\phi}{\left[a^2\sin^2\phi+\left(a\cos\phi-\delta\right)^2\right]^n}d\theta d\phi\,.$$

Since the integrand in this case is independent of θ, this integration can be effected immediately, and then by reorganising the denominator we may derive

$$I=2\pi a^2\int_0^{\pi}\frac{\sin\phi}{\left[a^2\sin^2\phi+\left(a\cos\phi-\delta\right)^2\right]^n}d\phi\,, \tag{6}$$

which by making the substitution $t=\delta^2+a^2-2\delta a\cos\phi$, becomes

$$\begin{aligned} I &= \frac{\pi a}{\delta}\int_{(\delta-a)^2}^{(\delta+a)^2}\frac{dt}{t^n} \\ &= \frac{\pi a}{\delta(n-1)}\left[\frac{1}{(\delta-a)^{2(n-1)}}-\frac{1}{(\delta+a)^{2(n-1)}}\right]. \end{aligned}$$

Therefore, the total interaction energy for a point and a sphere is given by

$$E_s = \frac{\pi a \eta}{\delta}\left\{-\frac{A}{2}\left[\frac{1}{(\delta-a)^4}-\frac{1}{(\delta+a)^4}\right]+\frac{B}{5}\left[\frac{1}{(\delta-a)^{10}}-\frac{1}{(\delta+a)^{10}}\right]\right\}, \qquad (7)$$

where η is the atomic surface density of the sphere.

An alternative approach

To demonstrate the utility of the hypergeometric function to evaluate these integrals and also to derive an expression which will be of use later, we now repeat the calculation of the integral (6) using hypergeometric functions. The method is to express this integral as

$$I = 2\pi a^2 \int_0^{\pi} \frac{2\sin(\phi/2)\cos(\phi/2)}{\left[(\delta-a)^2+4\delta a\sin^2(\phi/2)\right]^n} d\phi,$$

by making use of the trigonometric identities $1-\cos\phi = 2\sin^2(\phi/2)$ and $\sin\phi = 2\sin(\phi/2)\cos(\phi/2)$. We now make the substitution $t = \sin^2(\phi/2)$ and take out a factor of $2(\delta-a)^{-2n}$, which produces

$$I = \frac{4\pi a^2}{(\delta-a)^{2n}} \int_0^1 \left[1+\frac{4\delta a}{(\delta-a)^2}t\right]^{-n} dt.$$

This integral is in the form of the hypergeometric integral, and therefore

$$I = \frac{4\pi a^2}{(\delta-a)^{2n}} F\left(n,1;2;\frac{4\delta a}{(\delta-a)^2}\right).$$

At this point we may use a quadratic transformation, and in this case we may deduce

$$I = \frac{4\pi a^2}{\left(\delta^2 - a^2\right)^n} F\left(n, 2-n; \frac{3}{2}; \frac{a^2}{\delta^2 - a^2}\right),$$

and because the hypergeometric function is symmetric in *a* and *b* that this may be transformed into a Chebyshev polynomial of the second kind $U_n(x)$, which leads to the expression

$$I = \frac{4\pi a^2}{(n-1)\left(\delta^2 - a^2\right)^n} U_{n-2}\left(\frac{\delta^2 + a^2}{\delta^2 - a^2}\right),$$

Therefore the total interaction energy for a point and a sphere is also given by

$$E_s = 4\pi a^2 \eta \left[-\frac{A}{2\left(\delta^2 - a^2\right)^3} U_1\left(\frac{\delta^2 + a^2}{\delta^2 - a^2}\right) + \frac{B}{5\left(\delta^2 - a^2\right)^6} U_4\left(\frac{\delta^2 + a^2}{\delta^2 - a^2}\right) \right], \qquad (8)$$

where η is the atomic surface density of the sphere. We comment that equations (7) and (8) are precisely algebraically equivalent. However, the relationship to Chebyshev polynomials (which is not apparent in (7)) emerges naturally from the hypergeometric approach, where the relationships between the various transcendental functions and orthogonal polynomials can be readily accessed.

❖ **Interaction of two concentric spheres**

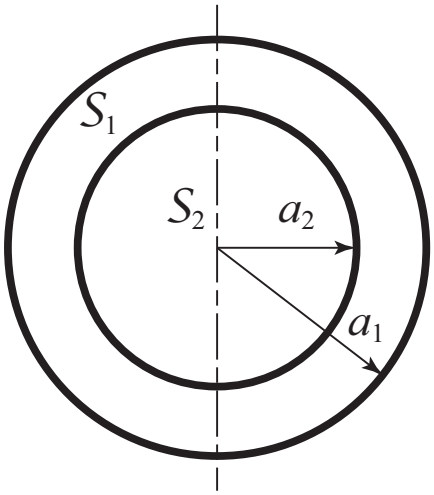

Fig. 4. Two interacting concentric spheres $\mathbf{S_1}$ and $\mathbf{S_2}$ of radii a_1 and a_2, respectively.

In this problem we have two spheres $\mathbf{S_1}$ and $\mathbf{S_2}$ with radii of a_1 and a_2, respectively, and with both spheres centred at the origin, as shown in Fig. 4. The first sphere has the spherical coordinates $\mathbf{S_1}(\theta,\phi)=(a_1,\theta,\phi)$. Here we employ the formula for the interaction of a point and sphere E_s, given in (8) and replace *a* by a_2 and δ by the distance from the centre of $\mathbf{S_2}$ to the typical surface element on $\mathbf{S_1}$, which in this case is simply $\delta=a_1$. This expression is then integrated over the surface of $\mathbf{S_1}$, which gives

$$E_{ssc}=4\pi a^2\eta_2\left[-\frac{A}{2\left(a_1^2-a_2^2\right)^3}U_1(\gamma)+\frac{B}{5\left(a_1^2-a_2^2\right)^3}U_4(\gamma)\right]\times\eta_1\int_0^{\pi}\int_{-\pi}^{\pi}a_1^2\sin\phi d\theta d\phi,$$

where $\gamma=\left(a_1^2+a_2^2\right)/\left(a_1^2-a_2^2\right)$ and in this case the integration is trivial and therefore we may immediately write

$$E_{ssc}=16\pi^2a_1^2a_2^2\eta_1\eta_2\left[-\frac{A}{2\left(a_1^2-a_2^2\right)^3}U_1(\gamma)+\frac{B}{5\left(a_1^2-a_2^2\right)^6}U_4(\gamma)\right], \tag{9}$$

where η_1 and η_2 are the atomic surface densities for spheres $\mathbf{S_1}$ and $\mathbf{S_2}$, respectively.

❖ Interaction of a sphere with an infinite cylinder

We now to consider a situation of considerable practical interest, which is that of the interaction between a sphere and a cylinder of infinite extent. In performing this calculation we take the sphere to be of radius *a* and centred at $(\varepsilon,0,0)$. The cylinder is taken to be of radius *b* and centred on the *z*-axis, such that in Cartesian coordinates the surface has the parametric form $(b\cos\theta,b\sin\theta,z)$, where $\theta\in(-\pi,\pi]$ and $z\in(-\infty,\infty)$. Therefore the distance between the centre of the sphere and a typical surface element on the cylinder is given by

$$\begin{aligned}\delta^2&=(b\cos\theta-\varepsilon)^2+b^2\sin^2\theta+z^2\\&=(b-\varepsilon)^2+4\varepsilon b\sin^2(\theta/2)+z^2.\end{aligned}$$

We now take the interaction energy for a point interacting with a sphere E_s given in (8) which can be written as

$$E_s = 4\pi a^2 \eta \left(-\frac{A}{2} J_1 + \frac{B}{5} J_4 \right),$$

and

$$J_n = \frac{1}{\left(\delta^2 - a^2\right)^{n+2}} U_n \left(\frac{\delta^2 + a^2}{\delta^2 - a^2} \right),$$

where $U_n(x)$ is the Chebyshev polynomial of the second kind. To evaluate the integration of E_s over the surface of the cylinder we may express J_n using the explicit formula for Chebyshev polynomials, which yields

$$\begin{aligned} J_n &= \frac{1}{\left(\delta^2 - a^2\right)^{n+2}} \sum_{m=0}^{\lfloor n/2 \rfloor} (-1)^m \binom{n-m}{m} 2^{n-2m} \left(\frac{\delta^2 + a^2}{\delta^2 - a^2} \right)^{n-2m} \\ &= \frac{1}{\left(\delta^2 - a^2\right)^{n+2}} \sum_{m=0}^{\lfloor n/2 \rfloor} (-1)^m \binom{n-m}{m} 2^{n-2m} \left(1 + \frac{2a^2}{\delta^2 - a^2} \right)^{n-2m} \\ &= \frac{1}{\left(\delta^2 - a^2\right)^{n+2}} \sum_{m=0}^{\lfloor n/2 \rfloor} (-1)^m \binom{n-m}{m} 2^{n-2m} \sum_{l=0}^{n-2m} \binom{n-2m}{l} \left(\frac{2a^2}{\delta^2 - a^2} \right)^l, \end{aligned}$$

which reduces the terms involving δ to be of the form $\left(\delta^2 - a^2\right)^{-k}$, where *k* is a positive integer and in particular we find

$$\begin{aligned} J_1 &= \frac{2}{\left(\delta^2 - a^2\right)^3} + \frac{4a^2}{\left(\delta^2 - a^2\right)^4}, \\ J_4 &= \frac{5}{\left(\delta^2 - a^2\right)^6} + \frac{80a^2}{\left(\delta^2 - a^2\right)^7} + \frac{336a^4}{\left(\delta^2 - a^2\right)^8} + \frac{512a^6}{\left(\delta^2 - a^2\right)^9} + \frac{256a^8}{\left(\delta^2 - a^2\right)^{10}}. \end{aligned}$$

Therefore we may deduce to evaluate the integral

$$I = b \int_{-\infty}^{\infty} \int_{-\pi}^{\pi} \frac{d\theta dz}{\left[\left(b - \varepsilon\right)^2 - a^2 + 4\varepsilon b \sin^2(\theta/2) + z^2 \right]^n},$$

where $n \in \{3, 4, 6, 7, 8, 9, 10\}$. We begin by defining $\lambda^2 = \left(b - \varepsilon\right)^2 - a^2 + 4\varepsilon b \sin^2(\theta/2)$, and then we make the substitution $z = \lambda \tan\psi$, which gives

$$I = b\int_{-\pi/2}^{\pi/2}\cos^{2n-2}\psi d\psi\int_{-\pi}^{\pi}\frac{1}{\lambda^{2n-1}}d\theta$$
$$= bB\left(n-1/2,1/2\right)\int_{-\pi}^{\pi}\frac{1}{\lambda^{2n-1}}d\theta,$$

where we $B\left(x,y\right)$ is the beta function. Now on making the further substitution $t=\sin^2(\theta/2)$, yields

$$I = \frac{2b}{\left[\left(b-\varepsilon\right)^2-a^2\right]^{n-1/2}}B\left(n-1/2,1/2\right)\int_0^1\frac{\left(1-\mu t\right)^{1/2-n}}{t^{1/2}\left(1-t\right)^{1/2}}dt,$$

where $\mu=-4b\varepsilon\left(b-\varepsilon\right)^2$. This integral is now in the Euler form, and we have

$$I = \frac{2b}{\left[\left(b-\varepsilon\right)^2-a^2\right]^{n-1/2}}B\left(n-1/2,1/2\right)\frac{\Gamma(1/2)\Gamma(1/2)}{\Gamma(1)}F\left(n-1/2,1/2;1;\mu\right)$$
$$= \frac{2\pi b}{\left[\left(b-\varepsilon\right)^2-a^2\right]^{n-1/2}}B\left(n-1/2,1/2\right)F\left(n-\frac{1}{2},\frac{1}{2};1;\frac{4\varepsilon b}{\left(b-\varepsilon\right)^2-a^2}\right).$$

It may be shown that

$$B\left(n-1/2,1/2\right)=\frac{\pi\left(2n-3\right)!!}{(2n-2)!!},$$

where !! is the double factorial operator such that $\left(2n-1\right)!!=(2n-1)(2n-3)(2n-5)\ldots$ and $\left(2n\right)!!=2n(2n-2)(2n-4)\cdots4\cdot2$. Simplify and collecting terms we may expresses the interaction energy between a sphere and a cylinder by

$$E_{sc}=8\pi^3a^2b\eta_1\eta_2\left[-\frac{A}{2}\left(2I_3+4a^2I_4\right)+\frac{B}{5}\left(5I_6+80a^2I_7+336a^4I_8+512a^6I_9+256a^8I_{10}\right)\right]$$

,

and

$$I_n=\frac{\left(2n-3\right)!!}{\left(2n-2\right)!!\left[\left(b-\varepsilon\right)^2-a^2\right]^{n-1/2}}F\left(n-\frac{1}{2},\frac{1}{2};1;\frac{4\varepsilon b}{\left(b-\varepsilon\right)^2-a^2}\right),$$

where η_1 and η_2 are the atomic surface densities for the cylinder and the sphere.

Output ที่ได้จากโครงการ

N. Thamwattana, **D. Baowan** and B. J. Cox (2013) Modelling bovine serum albumin inside carbon nanotubes, Royal Society of Chemistry (RSC) Advances, Vol. 3, pp. 23482-23488. (IF 2013: 3.708)

D. Baowan and N. Thamwattana (2014) Modelling encapsulation of gold and silver nanoparticles inside lipid nanotubes, Physica A: Statistical Mechanics and its Applications, Vol. 396, pp. 149-154. (IF 2013: 1.722)

D. Baowan and V. Helms (2014) Quantitative study of BSA coating silica nanoparticle, Journal of Mathematical Chemistry, Vol. 53, pp. 29-40. (IF 2013: 1.270)

D. Baowan, B. J. Cox and J. M. Hill (2015) Instability of carbon nanoparticles interacting with lipid bilayers, Royal Society of Chemistry (RSC) Advances, Vol. 15, pp. 5508-5515. (IF 2013: 3.708)

RSC Advances

RSC Publishing

PAPER

Modelling bovine serum albumin inside carbon nanotubes

Cite this: *RSC Adv.*, 2013, **3**, 23482

Ngamta Thamwattana,*[a] Duangkamon Baowan[bc] and Barry J. Cox[d]

Received 29th July 2013
Accepted 27th September 2013

DOI: 10.1039/c3ra43991g

www.rsc.org/advances

Bovine serum albumin is commonly used in many biochemical applications due to its stability, lack of interference within biochemical reactions and low production cost. Here, we model the interaction of bovine serum albumin inside a carbon nanotube. The carbon nanotube is chosen as an example to demonstrate its potential use in targeted drug and protein delivery and as an enzyme immobilizing material. We consider three possible structures as models for bovine serum albumin which are cylinder, prolate ellipsoid and three-connected spheres. Using the Lennard-Jones potential together with a continuum approach we obtain explicitly analytical expressions for the interaction energies of each configuration inside a carbon nanotube. These expressions are employed to determine the critical size of a nanotube which maximises the interaction with each model structure of the bovine serum albumin. Knowledge of the critical size is important and may be crucial for the design of a nanotube for maximum loading of the proteins and drug molecules.

1 Introduction

Bovine serum albumin (BSA) is a globular protein, which is used in many biochemical applications due to its stability and lack of interference within biochemical reactions. Further, the production cost of BSA is relatively low compared to other proteins commonly used in laboratory, since large quantities can be readily purified from bovine blood, a byproduct from the cattle industry. BSA is generally used in enzyme-linked immunosorbent assay (ELISA), immunoblots, and immunohistochemistry.[1–7] ELISA provides a highly sensitive procedure for quantitating antigens and antibodies.[1,2] BSA and protein Tween 20 are most often used to block vacant binding sites in ELISA.[3] Immunoblotting (or western blotting) is a rapid and sensitive assay for the detection and characterization of proteins that works by exploiting the specificity inherent in antigen–antibody recognition.[4,5] Immunohistochemical staining is a tool for detecting specific antigens in tissue.[6,7] Further, BSA is applied to many laboratory molecular techniques, including restriction enzyme digestions of DNA to increase thermal stability and half-life of the restriction enzymes in the reactions.[8] BSA is also commonly used to determine the quantity of other proteins, by comparing an unknown quantity of protein to known amounts of BSA.[9] Also, BSA can further enhance the effects of organic solvents on increased yield of polymerase chain reaction of GC-rich templates.[10] Lang[11] finds that the H/anti-H reaction in routine ABO bloodstain grouping can be enhanced by incorporating a suitable amount of BSA.

In terms of the geometry and structure of BSA, a number of experiments reports the shape of BSA to be a prolate ellipsoid of revolution with the dimensions of 140 Å for the major axis and 40 Å for the minor axis (Fig. 1b).[12,13] Other models for BSA

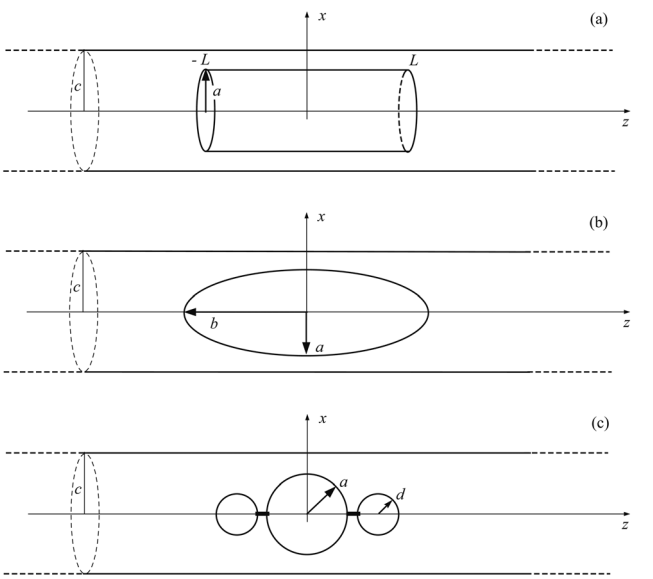

Fig. 1 Three possible configurations of bovine serum albumin inside a carbon nanotube: (a) cylinder, (b) prolate ellipsoid and (c) three-connected spheres.

[a]*Institute for Mathematics and Its Applications, School of Mathematics and Applied Statistics, University of Wollongong, NSW 2522, Australia. E-mail: ngamta@uow.edu.au*

[b]*Department of Mathematics, Faculty of Science, Mahidol University, Rama VI Rd, Bangkok 10400, Thailand*

[c]*Centre of Excellence in Mathematics, CHE, Si Ayutthaya Rd, Bangkok 10400, Thailand*

[d]*Nanomechanics Group, School of Mathematical Sciences, University of Adelaide, SA 5005, Australia*

This journal is © The Royal Society of Chemistry 2013

include spherical subunit models which comprise one large sphere and two or three identical smaller spheres aligned in a linear chain.[13,14] As an example, we only consider the subunit model that comprises three-connected spheres (Fig. 1(c)), noting that the mathematical formulation presented here can be easily extended to other spherical subunit models. The dimer of BSA is also studied through the subunit model of three-connected spheres.[13] In this paper, following ref. 12–14 we examine typical models of BSA, namely the prolate ellipsoid and the three-connected spheres. Additionally, motivated by the long length of BSA we propose a new model here, which is the cylindrical structure (Fig. 1(a)). We note that the secondary structure of BSA mainly comprises α-helix,[15,16] and as such BSA may be viewed as a cylindrical tubular structure.

The present paper examines the scenario where BSA is assumed to be immobilized inside a carbon nanotube. In their study, enzymes are generally immobilized on a solid support to improve their stability.[17] This immobilization of proteins and enzymes can prevent the rapid loss of biocatalytic effectiveness during the operation and storage periods resulting from autolysis effect, protein unfolding and aggregation. Among various nanomaterials (such as nanopores, nanofibers and nanotubes) carbon nanotubes are considered a promising material for enzyme immobilization research.[18–20] According to ref. 18 and 19, immobilization of enzymes in a carbon nanotube can occur through noncovalent and covalent conjugations. Noncovalent attachment generally preserves the unique properties of both enzymes and carbon nanotubes, but the immobilized protein can leak and gradually disappear during the use of the nanotube–enzyme complex. Covalent conjugation provides durable attachment, but the enzyme structure may be more disrupted. The main goal is to create the stable attachment of enzymes that maintains as much as possible the activity and function of their native state. In this paper, we consider the noncovalent conjugation or the adsorption of BSA in carbon nanotubes. Since the immobilized enzymes prepared by adsorption tend to leak from the carriers, owing to the relatively weak interaction between the enzyme and the carrier,[21] this paper predicts the critical size of carbon nanotubes which optimizes the interaction between BSA and a carbon nanotube, giving rise to the carbon nanotube–BSA complex that is most stable and minimises loss and leakage.

In addition to enzyme immobilization, carbon nanotubes represent a new class of molecular transporters that are potentially useful for *in vitro* and *in vivo* protein delivery applications.[22,23] In particular, Kam *et al.*[22] show the intracellular transport of various types of proteins (streptavidin, protein A, BSA and cytochrome c) that are non-covalently and non-specifically bound to the sidewalls of single-walled carbon nanotubes. Furthermore, Ge *et al.*[24] find that the interaction of blood proteins (such as BSA, Tf, BFG and Ig) with single-walled carbon nanotubes can greatly alter their cellular interaction pathways which results in much reduced cytotoxicity for nanotubes coated with these proteins. Other studies such as ref. 25 and 26 also examine the adsorption/desorption of BSA on carbon nanotubes for biomedical applications. While ref. 22–26 concern the adsorption of BSA onto the external surface of the nanotubes, Kharlamova *et al.*[27] study the adsorption of BSA inside carbon nanotubes. We note that in ref. 27 the diameters of carbon nanotubes studied are quite large which are in the range of 20–180 nm and as such large amount of BSA molecules are able to adsorb at the internal surface of the carbon nanotubes. In this paper, we only examine the interaction of a single BSA molecule inside a carbon nanotube. We determine the dimension of the nanotube that allows the acceptance of the BSA molecule from rest and also the critical radius of the nanotube that gives rise to the most stable structure of BSA–carbon nanotube complex.

In the next section, we briefly introduce the Lennard-Jones potential and a continuum approach which are used to determine the interaction between BSA and carbon nanotubes. Also, in Section 2, we propose mathematical models for three possible configurations of BSA, which are cylinder, prolate ellipsoid and three-connected spheres. Numerical results are presented in Section 3 and a summary of the paper follows in Section 4.

2 Modelling approach

In this paper, we assume that the adsorption of BSA in carbon nanotubes is attributed to a process generally referred to as physical adsorption, or physisorption, mediated by van der Waals forces. To model the van der Waals interaction between BSA and a carbon nanotube we use the Lennard-Jones potential and a continuum approach. The Lennard-Jones potential is given by

$$\Phi(\rho) = -\frac{A}{\rho^6} + \frac{B}{\rho^{12}},$$

where ρ denotes the distance between two atoms, A and B are the attractive and repulsive constants, respectively. For simplicity, we assume the isoelectric point (pH associated with zero net charge) for BSA,[28] so that we may neglect the electrostatic energy in the present model. We comment that a system comprising carbon nanotubes and BSA considered here contains large amount of atoms. Thus, using molecular dynamics or atomistic modelling for this system would be computationally expensive. Through our approach we obtain analytical results, which is computational efficiency, even though we sacrifice some accuracy. However, we note in many areas the sacrifice is justified as the model captures the dominant interactions.

We model the interaction of BSA inside a carbon nanotube, where we consider three possible structures as models of BSA, which are a cylinder, a prolate ellipsoid and a chain of three-connected spheres, as shown in Fig. 1. The dimensions for each model are given in Table 1. Note that the dimensions for the ellipsoid and the spherical subunit models are obtained from ref. 12–14, whereas we assume the same radial and axial lengths to that of ellipsoid for the cylindrical model.

Table 1 Dimensions for each model configuration of BSA

Cylinder	$a = 20$ Å	$L = 70$ Å
Prolate ellipsoid[12,13]	$a = 20$ Å	$b = 70$ Å
Three-connected spheres[14]	$a = 26.6$ Å	$d = 19.0$ Å

As shown in Fig. 1, we assume that the centre of the protein is located at the origin, which is also the centre of the carbon nanotube which is assumed to be of infinite length. To obtain the interaction energy for each configuration in Fig. 1, we first need to determine the energy between an atom at point **P** inside an infinite nanotube as shown in Fig. 2. Subsequently, we will assume that this atom is within the volume of BSA.

With reference to Cartesian coordinate system, a cylindrical nanotube of radius c can be parameterized by $(c\cos\theta, c\sin\theta, z)$, where $-\pi < \theta \leq \pi$ and $-\infty < z < \infty$. Next, we assume that the atom at point **P** has coordinates $(\delta, 0, 0)$, where $0 \leq \delta < c$. Therefore, the distance from point **P** to a typical surface element of the carbon nanotube is given by

$$\begin{aligned}\rho^2 &= (c\cos\theta - \delta)^2 + c^2\sin^2\theta + z^2 \\ &= \delta^2 + c^2 - 2\delta c\cos\theta + z^2 \\ &= (c-\delta)^2 + 4\delta c\sin^2(\theta/2) + z^2.\end{aligned} \tag{1}$$

Using a continuum approach, where atoms at discrete locations on the nanotube are averaged over its surface, the interaction energy between the atom at point **P** and the nanotube can be obtained by performing a surface integral of the Lennard-Jones potential over the nanotube, namely

$$E_a = \eta_c\int_S\left(-\frac{A}{\rho^6}+\frac{B}{\rho^{12}}\right)\mathrm{d}S = \eta_c(-AI_3 + BI_6), \tag{2}$$

where η_c represents the mean surface density of atoms on the nanotube. The integral I_n $(n = 3, 6)$ is defined by

$$I_n = \int_s \rho^{-2n}\mathrm{d}S. \tag{3}$$

Thus, from (1) and (3), we need to evaluate the following integrals

$$I_n = c\int_{-\infty}^{\infty}\int_{-\pi}^{\pi}\frac{1}{\left[(c-\delta)^2 + 4\delta c\sin^2(\theta/2) + z^2\right]^n}\mathrm{d}\theta\mathrm{d}z. \tag{4}$$

By introducing $\lambda^2 = (c-\delta)^2 + 4\delta c\sin^2(\theta/2)$ and substituting $z = \lambda\tan\psi$ into (4) we obtain

$$\begin{aligned}I_n &= c\int_{-\pi/2}^{\pi/2}\cos^{2n-2}\psi\mathrm{d}\psi\int_{-\pi}^{\pi}\frac{1}{\lambda^{2n-1}}\mathrm{d}\theta \\ &= cB(n-1/2,1/2)\int_{-\pi}^{\pi}\frac{1}{\lambda^{2n-1}}\mathrm{d}\theta,\end{aligned}$$

where $B(x, y)$ denotes the beta function. Upon using $t = \sin^2(\theta/2)$ yields

$$I_n = \frac{2c}{(c-\delta)^{2n-1}}B(n-1/2,1/2)\int_0^1 t^{-1/2}(1-t)^{-1/2}(1-\mu t)^{1/2-n}\mathrm{d}t,$$

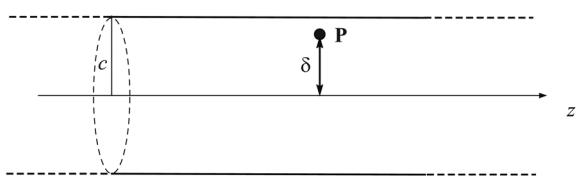

Fig. 2 A nanotube of radius c interacting with an interior atom at point **P** offsetting from the central axis by a distance δ.

where $\mu = -4c\delta/(c-\delta)^2$. The above integral is now in the Euler form, which from

$$F(\alpha,\beta;\gamma;z) = \frac{\Gamma(\gamma)}{\Gamma(\beta)\Gamma(\gamma-\beta)}\int_0^1 t^{\beta-1}(1-t)^{\gamma-\beta-1}(1-tz)^{-\alpha}\mathrm{d}t,$$

we have

$$\begin{aligned}I_n &= \frac{2c}{(c-\delta)^{2n-1}}B(n-1/2,1/2)\frac{\Gamma(1/2)\Gamma(1/2)}{\Gamma(1)}F(n-1/2,1/2;1;\mu) \\ &= \frac{2\pi c}{(c-\delta)^{2n-1}}B(n-1/2,1/2)F(n-1/2,1/2;1;\mu),\end{aligned}$$

where $\Gamma(x)$ represents the gamma function and $F(\alpha, \beta; \gamma, z)$ denotes the usual hypergeometric function. Since we have here that $\gamma = 2\beta$, we may employ the quadratic transformation

$$\begin{aligned}F(\alpha,\beta;2\beta;z) = &\left[\frac{1+(1-z)^{1/2}}{2}\right]^{-2\alpha} \\ &\times F\left(\alpha,\alpha-\beta+1/2;\beta+1/2;\left[\frac{1-(1-z)^{1/2}}{1+(1-z)^{1/2}}\right]^2\right),\end{aligned}$$

which gives

$$\begin{aligned}I_n &= \frac{2\pi c}{(c-\delta)^{2n-1}}B(n-1/2,1/2)\left(\frac{c-\delta}{c}\right)^{2n-1} \\ &\quad\times F\left(n-1/2,n-1/2;1;\delta^2/c^2\right) \\ &= \frac{2\pi}{c^{2n-2}}B(n-1/2,1/2)F\left(n-1/2,n-1/2;1;\delta^2/c^2\right).\end{aligned}$$

By expanding the hypergeometric function using the series representation, we obtain

$$I_n = \frac{2\pi}{c^{2n-2}}B(n-1/2,1/2)\sum_{m=0}^{\infty}\left(\frac{(n-1/2)_m\delta^m}{m!\,c^m}\right)^2, \tag{5}$$

where $(a)_m$ is the Pochhammer symbol. By substituting (5) into (2) we obtain the interaction energy E_a between a carbon nanotube and an internal atom.

Next, we assume that the atom at point **P** is within the volume element of BSA. As such, we may determine the molecular interaction arising from the BSA by performing a volume integral of E_a over the volume of the protein, namely

$$E_s = \eta_s\int_v E_a(\delta)\mathrm{d}V = \eta_s\eta_c\int_v(-AI_3(\delta) + BI_6(\delta))\mathrm{d}V, \tag{6}$$

where I_n is given by (5), δ is the distance from the nanotube axis to a typical volume element of the protein and η_s is the mean volume density of BSA, which depends on the assumed configuration of the protein. As such, we may write (6) as

$$E_s = \eta_s\eta_c(-AK_3 + BK_6), \tag{7}$$

where the integral K_n is given by

$$K_n = \int_v I_n(\delta)\mathrm{d}V. \tag{8}$$

This journal is © The Royal Society of Chemistry 2013

Based on (5), to find K_n we need to evaluate the integral of the form

$$J_m = \int_v \delta^{2m} \mathrm{d}V, \tag{9}$$

where m is a nonnegative integer appearing in the summation from (5).

In the following subsections, we examine the three proposed model configurations for a BSA molecule, namely cylinder, prolate ellipsoid and three-connected spheres, and perform the volume integral (9) according to the geometry of each configuration.

2.1 Cylindrical model

Here we model the BSA as a cylinder centred at the origin with radius a and length $2L$, as shown in Fig. 1(a). In a rectangular coordinate system, a typical point in the cylinder can be parameterized by ($ar\cos\theta$, $ar\sin\theta$, z) where $0 \le r \le 1$, $-\pi \le \theta \le \pi$ and $-L \le z \le L$. Therefore, in this case the distance δ is given by $\delta^2 = a^2r^2$, and the volume element is $\mathrm{d}V = a^2r\mathrm{d}r\mathrm{d}\theta\mathrm{d}z$. As a result, we have

$$\begin{aligned} J_m &= \int_{-L}^{L}\int_{-\pi}^{\pi}\int_0^1 a^{2m+2}r^{2m+1}\mathrm{d}r\mathrm{d}\theta\mathrm{d}z \\ &= 4\pi L a^{2m+2}\int_0^1 r^{2m+1}\mathrm{d}r \\ &= \frac{4\pi L a^{2m+2}}{2m+2}. \end{aligned} \tag{10}$$

On using a relation between a beta function and a gamma function, we have

$$J_m = \frac{2\pi L a^{2m+2} m!}{(2)_m}.$$

Thus, from (5) and (8) we obtain

$$\begin{aligned} K_n &= \frac{4\pi^2 a^2 L}{c^{2n-2}} B(n-1/2,1/2)\sum_{m=0}^{\infty}\frac{(n-1/2)_m(n-1/2)_m}{(2)_m m!}\left(\frac{a^2}{c^2}\right)^m \\ &= \frac{4\pi^2 a^2 L}{c^{2n-2}} B(n-1/2,1/2)F\left(n-1/2,n-1/2;2;a^2/c^2\right). \end{aligned} \tag{11}$$

Upon substituting (11) into (7) we may obtain the interaction energy of a cylindrical shaped BSA situated inside a carbon nanotube.

2.2 Prolate ellipsoidal model

Now we analyse a prolate spheroid with the axis of rotation collinear with the z-axis and centred at the origin. The equatorial semi-axes have length a and the polar semi-axis (along the z-axis) has length b. The relation between the spheroidal and rectangular coordinates is given by

$$x = ar\sin\phi\cos\theta,\ y = ar\sin\phi\sin\theta,\ z = br\cos\phi, \tag{12}$$

where $0 \le r \le 1$, $0 \le \phi \le \pi$ and $-\pi < \theta \le \pi$. Then the offset distance δ is given by $\delta^2 = a^2r^2\sin^2\phi$. Further, the volume element of the spheroid is $\mathrm{d}V = a^2br^2\sin\phi\mathrm{d}r\mathrm{d}\phi\mathrm{d}\theta$. Hence, we may deduce

$$\begin{aligned} J_m &= \int_{-\pi}^{\pi}\int_0^{\pi}\int_0^1 a^{2m+2}br^{2m+2}\sin^{2m+1}\phi\mathrm{d}r\mathrm{d}\phi\mathrm{d}\theta \\ &= 2\pi a^{2m+2}b\int_0^{\pi}\sin^{2m+1}\phi\mathrm{d}\phi\int_0^1 r^{2m+2}\mathrm{d}r \\ &= \frac{2\pi a^{2m+2}b}{2m+3}B(m+1,1/2). \end{aligned} \tag{13}$$

Again on using a relation between a beta function and a gamma function, we have

$$J_m = \frac{4\pi a^{2m+2}bm!}{3(5/2)_m}.$$

Thus, from (5) and (8) we find

$$\begin{aligned} K_n &= \frac{8\pi^2 a^2 b}{3c^{2n-2}}B(n-1/2,1/2)\sum_{m=0}^{\infty}\frac{(n-1/2)_m(n-1/2)_m}{(5/2)_m m!}\left(\frac{a^2}{c^2}\right)^m \\ &= \frac{8\pi^2 a^2 b}{3c^{2n-2}}B(n-1/2,1/2)F\left(n-1/2,n-1/2;5/2;a^2/c^2\right), \end{aligned} \tag{14}$$

which upon substituting into (7), we can obtain the interaction energy of an ellipsoidal BSA inside a carbon nanotube.

2.3 Model of three-connected spheres

Here, we model BSA as a structure comprising three-connected spheres in a linear chain. We assume that the largest sphere has radius a and that its centre is located at the origin. The two other spheres are assumed to locate on each side of the largest sphere and each has radius d. We note that we do not need to consider the interaction between each sphere here, since we assume that the molecule is at equilibrium.

To obtain the interaction energy for a sphere of radius a inside a nanotube, we simply use the result from the previous section, whereby we substitute $b = a$ in the integral K_n (14) to obtain

$$\begin{aligned} K_n &= \frac{8\pi^2 a^3}{3c^{2n-2}}B(n-1/2,1/2)\sum_{m=0}^{\infty}\frac{(n-1/2)_m(n-1/2)_m}{(5/2)_m m!}\left(\frac{a^2}{c^2}\right)^m \\ &= \frac{8\pi^2 a^3}{3c^{2n-2}}B(n-1/2,1/2)F\left(n-1/2,n-1/2;5/2;a^2/c^2\right). \end{aligned} \tag{15}$$

For the sphere of radius d, we may replace a by d in (15) to obtain K_n which by substituting into (7) we can obtain the interaction energy for a sphere of radius d inside a nanotube. As such the total energy for the BSA assuming to have the structure of three-connected spheres situated inside a carbon nanotube is given by

$$E_{\mathrm{tot}} = E_{\mathrm{s}}(a) + 2E_{\mathrm{s}}(d). \tag{16}$$

3 Numerical results

In order to evaluate the interaction energy of a BSA inside a carbon nanotube, we need to determine the physical

parameters involved in the model. We note that there are 9684 atoms in a BSA molecule, comprising 3072 carbon, 4828 hydrogen, 816 nitrogen, 928 oxygen and 40 sulfur atoms. As a result we may determine the average attractive and repulsive constants between BSA interacting with a nanotube which is made up entirely of carbon atoms as

$$A = (3072A_{CC} + 4828A_{HC} + 816A_{NC} + 928A_{OC} + 40A_{SC})/9684,$$
$$B = (3072B_{CC} + 4828B_{HC} + 816B_{NC} + 928B_{OC} + 40B_{SC})/9684, \quad (17)$$

where A_{ij} and B_{ij} are the attractive and repulsive constants for atom i interacting with atom j. Using the van der Waals diameters σ and well-depths ε from Rappi *et al.*[29] for each atom type and then employing the empirical combing rules $\sigma_{ij} = (\sigma_i + \sigma_j)/2$ and $\varepsilon_{ij} = \sqrt{\varepsilon_i \varepsilon_j}$, we find the attractive and repulsive constants from $A_{ij} = 2\sigma_{ij}{}^6\varepsilon_{ij}$ and $B_{ij} = \sigma_{ij}{}^{12}\varepsilon_{ij}$ for the interaction between different type of atoms as shown in Table 2. As such, from (17) we obtain the values of A and B for BSA–carbon nanotube interaction as also given in Table 2. We note that the values of the van der Waals diameter and well-depth given in ref. 29 have been widely used in many research fields, including computational chemistry, physical chemistry and nanotechnology, and this work of Rappi *et al.* has been cited more than 1200 times.

We determine the atomic volume densities (η_s) for each configuration of BSA which can be found from dividing the total number of atoms in BSA by the volume of the assumed structure. For the cylinder model, $n_s = 9684/(2\pi La^2)$. For the prolate ellipsoid, we have $n_s = 9684/(4\pi a^2 b/3)$. For the model of three-connected spheres, all the segments are assumed to be of equal density,[14] and thus $\eta_s = 9684/(4\pi[a^3 + 2d^3]/3)$. We note that the values for a, b, d and L for each configuration are given in Table 1. For the atomic surface density of a carbon nanotube, we use $\eta_c = 0.3821$ Å^{-2} which is the same value to that of graphene.[30] The numerical values for all of the atomic densities used in this paper are given in Table 3.

Using MAPLE, we plot the interaction energy for the three configurations of BSA situated inside a carbon nanotube. We assume that the carbon nanotube has radius c and is infinite in length. In Fig. 3 we plot for each configuration the relationship

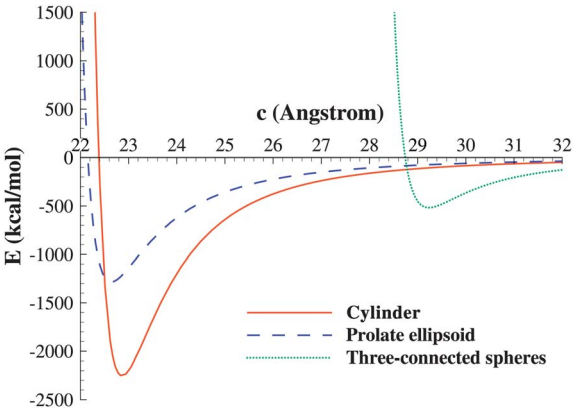

Fig. 3 Interaction energy for each configuration of bovine serum albumin inside a carbon nanotube of radius c.

between the interaction energy and the radius of a carbon nanotube. From this figure, we observe a similar trend for all configurations. The equilibrium position for BSA lies a certain distance away from the inner surface of the nanotube where the interaction energy is minimum. The critical radius for the nanotube which minimises the interaction energy for each configuration is prescribed in Table 4. From Fig. 3 we can also deduce the minimum radius of a carbon nanotube that will accept each model configuration of BSA molecule from rest (see Table 5). This result may be used to design a carbon nanotube to purify BSA from other proteins. For example, Sun *et al.*[31] use a carbon nanotube of radius 35 Å to separate protein lysozyme from BSA. If we assume a BSA molecule as a single sphere of radius 36 Å as suggested in ref. 31, then by using the result in Section 2.3 we find that the minimum radius which will accept the BSA molecule is 38.146 Å. Thus, this finding supports the study of ref. 31 where BSA is completely rejected from the carbon nanotube of radius 35 Å.

Furthermore, from Fig. 3 we can see that there is a significant difference in the energy level for the three proposed models of BSA. We note that the volumes of cylindrical, ellipsoidal and three-connected spherical BSAs are 175 929.1886, 117 286.1257 and 136 299.4466 Å^3, respectively. The cylinder has the largest volume which gives rise to the maximum binding energy with the carbon nanotube. Even though we assume a similar dimension for the cylinder and the prolate ellipsoid, the larger

Table 2 Numerical values of the attractive and repulsive constants

Interaction	A (Å^6 kcal mol^{-1})	B (Å^{12} kcal mol^{-1})
C–C	684.9524	1 117 047.196
H–C	198.5959	145 063.9865
N–C	477.5906	669 934.5728
O–C	391.3802	482 466.7624
S–C	1274.8544	2 395 472.866
BSA–carbon nanotube	399.3085	539 255.7407

Table 3 Numerical values for various atomic densities

Surface density of carbon nanotubes	$\eta_c = 0.3812$ Å^{-2}
Volume density of cylindrical BSA	$\eta_s = 0.0550$ Å^{-3}
Volume density of ellipsoidal BSA	$\eta_s = 0.0826$ Å^{-3}
Volume density of each unit of spherical BSA	$\eta_s = 0.0710$ Å^{-3}

Table 4 Critical radius of a carbon nanotube which optimizes the interaction with each model configuration of BSA

BSA	Cylinder	Ellipsoid	Three spheres
c (Å)	22.868	22.642	29.231

Table 5 Minimum radius of a carbon nanotube which accepts each model configuration of BSA

BSA	Cylinder	Ellipsoid	Three spheres
c (Å)	22.385	22.156	28.742

This journal is © The Royal Society of Chemistry 2013

ends of the cylinder require a slightly larger size of a carbon nanotube to accommodate the cylindrical BSA compared to that of the prolate ellipsoidal structure (see Table 4). For the model of three-connected spheres, the size of the nanotube is strongly dependent on the radius of the largest sphere. For all cases, we find that the shortest distances between the outer surface of the BSA and the inner surface of the nanotube are approximately 2.868, 2.642 and 2.631 Å for cylinder, prolate ellipsoid and three-connected spheres, respectively. We comment that the latter two models are more realistic as they are a closer match to experimental observation and therefore we find that the system is at equilibrium and most stabilized when the outer surface of BSA is at the distance approximately 2.6 Å away from the inner surface of a carbon nanotube. We note that this equilibrium spacing is also true for the case of the model configuration of BSA given in ref. 31 (*i.e.* a single sphere of radius 36 Å), where we find the critical radius of the nanotube to be 38.630 Å.

4 Summary

In this paper, we use the Lennard-Jones potential together with a continuum approach to model the interaction of a BSA molecule inside a carbon nanotube. Three model configurations of BSA are considered, which are cylinder, prolate ellipsoid and three-connected spheres. We find that the cylinder has the maximum binding energy followed by the ellipsoid and the three-connected spheres. The maximum binding energy depends directly on the volume of the model configuration.

Inside a nanotube, BSA adopts an equilibrium location that is a certain distance away from the inner surface of the nanotube where the energy is minimised. The equilibrium distance between the BSA and the nanotube strongly depends on the radial dimension of the model configuration of BSA. For the case of three-connected spheres, the radius of the largest sphere strongly influences the critical size of the nanotube which gives rise to the optimal complex. In Table 4 we prescribe the critical radius of the carbon nanotube which optimizes the interaction energy for each configuration of BSA. We note that even though the cylinder and the ellipsoid have the same width at the centre of the molecule, the cylinder requires a larger radius nanotube to accommodate the molecule. This is likely due to the larger ends of the cylinder as compared to those of the prolate ellipsoid.

We comment that a knowledge of the critical radius of nanotube which optimizes the interaction with BSA is important for the design of materials for effective proteins and enzymes immobilization. In ref. 28, BSA and lysozyme are employed as model proteins to investigate the loading and release efficiencies of titania nanotubes for use in drug delivery. We comment that the mathematical formulation given here can be easily applied to investigate the interaction of BSA with titania nanotubes and other types of nanopores and channels.

Acknowledgements

The authors acknowledge financial support from the University of Wollongong (UOW) and UOW's Internationalisation Linkage Grant Scheme. DB also acknowledges the Thailand Research Fund (TRG5680072).

References

1 M. F. Clark and A. N. Adams, Characteristics of the Microplate Method of Enzyme-Linked Immunosorbent Assay for the Detection of Plant Viruses, *J. Gen. Virol.*, 1977, **34**, 475–483.
2 H. Schønheyder and P. Andersen, Effects of bovine serum albumin on antibody determination by the enzyme-linked immunosorbent assay, *J. Immunol. Methods*, 1984, **72**, 251–259.
3 M. Steinitz, Quantitation of the Blocking Effect of Tween 20 and Bovine Serum Albumin in ELISA Microwells, *Anal. Biochem.*, 2000, **282**, 232–238.
4 E. Wedege and G. Svenneby, Effects of the blocking agents bovine serum albumin and Tween 20 in different buffers on immunoblotting of brain proteins and marker proteins, *J. Immunol. Methods*, 1986, **88**, 233–237.
5 J. A. Hinson, S. L. Michael, S. G. Ault and N. R. Pumford, Western Blot Analysis for Nitrotyrosine Protein Adducts in Livers of Saline-Treated and Acetaminophen-Treated Mice, *Toxicol. Sci.*, 2000, **53**, 467–473.
6 Y. Liu, P. Layrolle, J. de Bruijn, C. van Blitterswijk and K. de Groot, Biomimetic coprecipitation of calcium phosphate and bovine serum albumin on titanium alloy, *J. Biomed. Mater. Res.*, 2001, **57**, 327–335.
7 M. Shiota, J. Fujimoto, M. Takenaga, H. Satoh, R. Ichinohasama, M. Abe, M. Nakano, T. Yamamoto and S. Mori, Diagnosis of t(2;5)(p23;q35)-associated Ki-1 lymphoma with immunohistochemistry, *Blood*, 1994, **84**, 3648–3652.
8 C. A. Kreader, Relief of amplification inhibition in PCR with bovine serum albumin or T4 gene 32 protein, *Appl. Environ. Microbiol.*, 1996, **62**, 1102–1106.
9 T. Zor and Z. Selinger, Linearization of the Bradford protein assay increases its sensitivity: Theoretical and experimental studies, *Anal. Biochem.*, 1996, **236**, 302–308.
10 E. M. Farell and G. Alexandre, Bovine serum albumin further enhances the effects of organic solvents on increased yield of polymerase chain reaction of GC-rich templates, *BMC Res. Notes*, 2012, **5**, 257.
11 B. G. Lang, The use of bovine serum albumin for H antigen typing in bloodstains, *J. Forensic Sci. Soc.*, 1976, **16**, 61–66.
12 A. Kentwright and M. R. Thomson, Hydrodynamic structure of bovine serum albumin determined by transient electric birefringence, *Biophys. J.*, 1975, **15**, 137–141.
13 P. G. Squire, P. Moser and C. T. O'Konski, The hydrodynamic properties of bovine serum albumin monomer and dimer, *Biochemistry*, 1968, **7**, 4261–4272.
14 V. Bloomfield, The structure of bovine serum albumin at low pH, *Biochemistry*, 1966, **5**, 684–689.
15 R. G. Reed, R. C. Feldhoff, O. L. Clute and T. Peters Jr, Fragments of bovine serum albumin produced by limited proteolysis. Conformation and ligand binding, *Biochemistry*, 1975, **14**, 4578–4583.

16 A. D. McLachlan and J. E. Walker, Evolution of serum albumin, *J. Mol. Biol.*, 1977, **112**, 543–558.
17 N. Laurent, R. Haddoub and S. L. Flitsch, Enzyme catalysis on solid surfaces, *Trends Biotechnol.*, 2008, **26**, 328–337.
18 W. Feng and P. Ji, Enzymes immobilized on carbon nanotubes, *Biotechnol. Adv.*, 2011, **29**, 889–895.
19 N. Saifuddin, A. Z. Raziah and A. R. Junizah, Carbon nanotubes: A review on structure and their interaction with proteins, *J. Chem.*, 2013, **2013**, 676815.
20 L. Wang and R. Jiang, Reversible his-tagged enzyme immobilization on functionalized carbon nanotubes as nanoscale biocatalyst, *Methods Mol. Biol.*, 2011, **743**, 95–106.
21 M. M. M. Elnashar, The Art of Immobilization using Biopolymers, Biomaterials and Nanobiotechnology, http://www.intechopen.com/download/pdf/16195.
22 N. W. S. Kam and H. Dai, Carbon nanotubes as intracellular protein transporters: Generality and biological functionality, *J. Am. Chem. Soc.*, 2005, **127**, 6021–6026.
23 N. W. S. Kam, Z. Liu and H. Dai, Carbon nanotubes as intracellular transporters for proteins and DNA: An investigation of the uptake mechanism and pathway, *Angew. Chem.*, 2006, **118**, 591–595.
24 C. Ge, J. Dua, L. Zhaoa, L. Wanga, Y. Liua, D. Lia, Y. Yanga, R. Zhoub, Y. Zhaoa, Z. Chaid and C. Chena, Binding of blood proteins to carbon nanotubes reduces cytotoxicity, *Proc. Natl. Acad. Sci. U. S. A.*, 2011, **108**, 16968–16973.
25 L. E. Valenti, P. A. Fiorito, C. D. Garcia and C. E. Giacomelli, The adsorption–desorption process of bovine serum albumin on carbon nanotubes, *J. Colloid Interface Sci.*, 2007, **307**, 349–356.
26 X. Zhao, R. Liu, Z. Chi, Y. Teng and P. Qin, New insights into the behavior of bovine serum albumin adsorbed onto carbon nanotubes: Comprehensive spectroscopic studies, *J. Phys. Chem. B*, 2010, **114**, 5625–5631.
27 M. V. Kharlamova, V. N. Mochalin, M. R. Lukatskaya, J. Niu, V. Presser, S. Mikhalovsky and Y. Gogotsi, Adsorption of proteins in channels of carbon nanotubes: Effect of surface chemistry, *Mater. Express*, 2013, **3**, 1–10.
28 K. C. Popat, M. Eltgroth, T. J. LaTempa, C. A. Grimes and T. A. Desai, Titania nanotubes: A novel platform for drug-eluting coatings for medical implants?, *Small*, 2007, **3**, 1878–1881.
29 A. K. Rappi, C. J. Casewit, K. S. Colwell, W. A. Goddard III and W. M. Skid, UFF, a full periodic table force field for molecular mechanics and molecular dynamics simulations, *J. Am. Chem. Soc.*, 1992, **114**, 10024–10035.
30 N. Thamwattana and J. M. Hill, Continuum modelling for carbon and boron nitride nanostructures, *J. Phys.: Condens. Matter*, 2007, **19**, 406209.
31 X. Sun, X. Su, J. Wu and B. J. Hinds, Electrophoretic transport of biomolecules through carbon nanotube membranes, *Langmuir*, 2011, **27**, 3150–3156.

 This journal is © The Royal Society of Chemistry 2013

Provided for non-commercial research and education use.
Not for reproduction, distribution or commercial use.

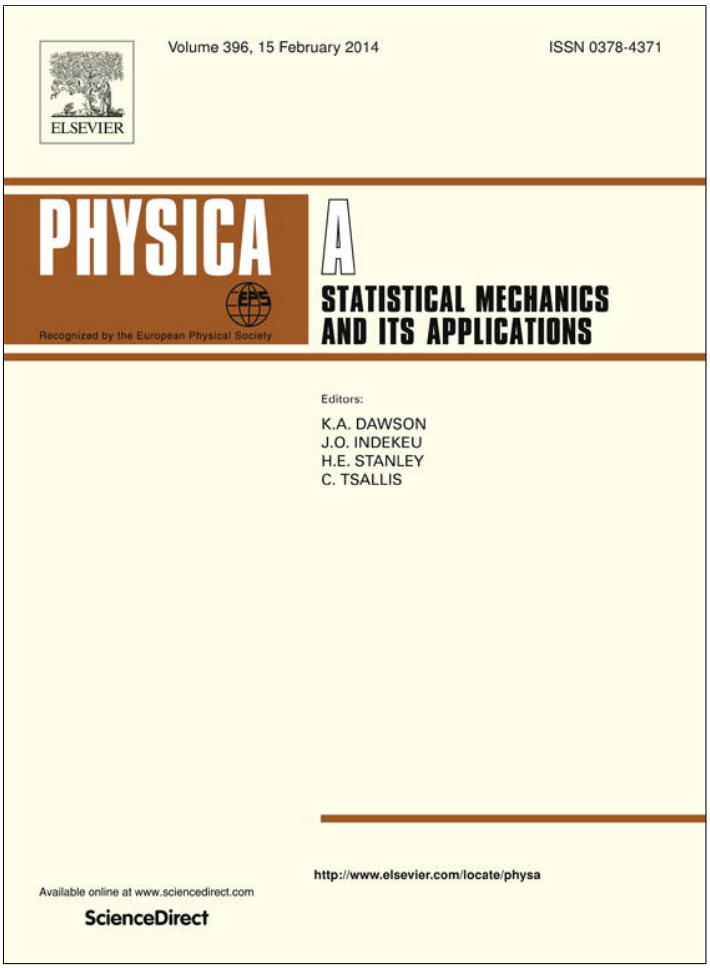

This article appeared in a journal published by Elsevier. The attached copy is furnished to the author for internal non-commercial research and education use, including for instruction at the authors institution and sharing with colleagues.

Other uses, including reproduction and distribution, or selling or licensing copies, or posting to personal, institutional or third party websites are prohibited.

In most cases authors are permitted to post their version of the article (e.g. in Word or Tex form) to their personal website or institutional repository. Authors requiring further information regarding Elsevier's archiving and manuscript policies are encouraged to visit:

http://www.elsevier.com/authorsrights

Author's personal copy

Physica A 396 (2014) 149–154

Contents lists available at ScienceDirect

Physica A

journal homepage: www.elsevier.com/locate/physa

Modelling encapsulation of gold and silver nanoparticles inside lipid nanotubes

Duangkamon Baowan [a,b,*], Ngamta Thamwattana [c]

[a] Department of Mathematics, Faculty of Science, Mahidol University, Rama VI, Bangkok 10400, Thailand

[b] Centre of Excellence in Mathematics, CHE, Si Ayutthaya Rd., Bangkok 10400, Thailand

[c] Institute for Mathematics and Its Applications, School of Mathematics and Applied Statistics, University of Wollongong, NSW 2522, Australia

HIGHLIGHTS

- Suction energies for gold and silver nanoparticles into lipid nanotubes are studied.
- Lennard-Jones potential and the continuous approximation are utilised.
- Surface and volume integrations are undertaken to evaluate analytical expressions.
- We predict the acceptance of gold and silver nanoparticles inside lipid nanotubes.

ARTICLE INFO

Article history:
Received 18 July 2013
Received in revised form 24 October 2013
Available online 18 November 2013

Keywords:
Lipid nanotubes
Gold
Silver
Encapsulation

ABSTRACT

Lipid nanotubes are of particular interest for use as a template to create various one-dimensional nanostructures and as a carrier for drug and gene delivery. Understanding the encapsulation process is therefore crucial for such development. This paper models the interactions between lipid nanotubes and spheres of gold and silver nanoparticles and determines the critical dimension of lipid nanotubes that maximises the interaction with the nanoparticles. Our results confirm the acceptance of gold and silver nanoparticles inside lipid nanotubes. Further, we find that the lipid nanotube of radius approximately 10.23 nm is most favourable to encapsulate both types of nanoparticles.

© 2013 Elsevier B.V. All rights reserved.

1. Introduction

Drug delivery is one of the most promising biomedical applications of nanotechnology [1]. The direct delivery of drugs and biomolecules into the cell has put the focus on the development of efficient and safe carriers to transport genes and drugs. A large number of nanoparticles could potentially be used for cellular delivery due to their versatile properties, including good biocompatibility, selective targeted delivery and controlled release of carried drugs. Currently, nanocarriers are being developed from a wide range of materials and amongst them lipid nanotubes are of particular interest.

Self-assembling from lipid molecules in liquid media, lipid nanotubes are open-ended, hollow cylindrical structures composed of rolled-up bilayer membrane walls [2]. Their special properties include controllable diameters and length and easily functionalisable both external and internal surfaces, giving rise to a potential use as template-synthesised one-dimensional molecular structures, such as nanotubes, concentric tubular hybrids, complex helical architectures and one-dimensional arrays of quantum dots [2]. Furthermore, lipid nanotubes can be employed as a nanocontainer for nanomaterials and biomolecules for applications in drug and gene delivery [2–4]. In particular, their advantages over other materials

* Corresponding author at: Department of Mathematics, Faculty of Science, Mahidol University, Rama VI, Bangkok 10400, Thailand. Tel.: +66 22015350.
E-mail address: duangkamon.bao@mahidol.ac.th (D. Baowan).

0378-4371/$ – see front matter © 2013 Elsevier B.V. All rights reserved.
http://dx.doi.org/10.1016/j.physa.2013.11.003

Author's personal copy

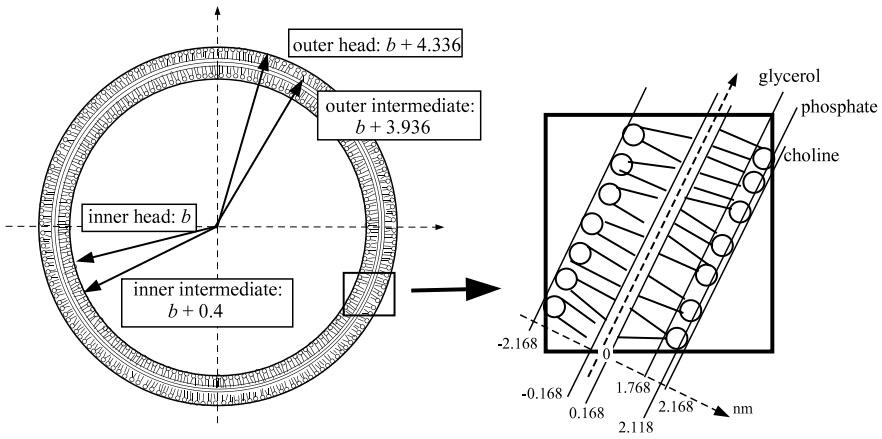

Fig. 1. Schematic diagram of a lipid nanotube illustrating its structural dimension.

include biocompatibility, accessibility to their inner surfaces, ability to functionalise outer surfaces, less vulnerable to microbial attack, large inner volume, controllability of their diameters, wall thickness and length, and ability to manipulate, position and align on diverse substrates with various techniques [2,4].

Lipid bilayer is a complex structure and many researchers attempt its modelling using a coarse grain approach [5–11]. The coarse grain model smooths over or averages a number of atoms. Marrink et al. [6,7] describe the parametrisation of the coarse grain model for the dipalmitoylphosphatidylcholine (DPPC) lipid system. Shelly et al. [8] suggest that a coarse grain model is more efficient to model the self-assembly of phospholipids compared to the Monte Carlo simulations. Using parameters from a coarse grain model [6,7], Baowan et al. [12] adopt the Lennard-Jones potential and a continuum approach to model the structure of lipid bilayer and the interaction between the lipid bilayer and a fullerene C_{60}. In Baowan et al. [12], the lipid bilayer is assumed to comprise the head group which is modelled as a flat plane and the tail group which is modelled as a rectangular box. Since lipid nanotubes are composed of rolled-up lipid bilayer membranes, following the concept in Ref. [12], here we assume six layers of a lipid nanotube as shown in Fig. 1, namely two head groups, two intermediate layers and two tail groups. The intermediate layer is assumed to be averaged over a cylindrical surface whereas the head group and the tail group are assumed to be averaged within cylinders of prescribed thicknesses.

As mentioned in Refs. [2–4], lipid nanotubes can be used to encapsulate gold and silver nanoparticles for creating nanowires. As such, this paper investigates the interactions between lipid nanotubes and spheres of gold and silver nanoparticles, and determines the critical dimension of lipid nanotubes that are favourable to selective encapsulation and controlled release of the nanoparticles. Gold nanoparticles have been comprehensively studied in biological and medical areas. Moreover, experiments have shown that mammalian cells can uptake gold nanoparticles [13]. In terms of structural study of the gold nanoparticles, Pu et al. [14] employ molecular dynamics simulations to stretch gold nanowires in solvents, and they conclude that the packing density of a gold surface is smaller than that in the system comprising the benzenedithiol solvent and the gold particles. Further, this paper also studies the encapsulation of silver nanoparticles into lipid nanotubes. Similar to gold, silver nanoparticles are of particular interest to various fields of applications, including anti-bacterial agents, bio-sensing, textile coatings, electronics, food storage, cosmetics and environmental applications [15,16]. Hosting gold and silver nanoparticles inside lipid nanotubes can generate nanowires and may yield further exciting applications, especially in the area of medicine. As such, understanding the interacting mechanisms among these nanostructures is crucial for future development.

In the following section, we introduce the Lennard-Jones potential and a continuum approach which are used to model the interaction between lipid nanotubes and gold and silver nanoparticles. Analytical evaluation of the interaction energy of lipid nanotubes and spherical nanoparticles is given in Section 3. In Section 4, numerical results for our model are provided and discussion of our findings are given.

2. Interaction energy

Here we introduce a simple model for the interaction between lipid nanotubes and gold and silver nanoparticles. As the electrostatic effect can be neglected [17], this model only takes into account the van der Waals interaction. We also make another assumption that gold and silver nanoparticles considered here are perfect spheres. We employ the Lennard-Jones potential and a continuum approximation to determine the molecular interatomic energy arising from the van der Waals interaction between a spherical nanoparticle and a lipid nanotube. The classical 6–12 Lennard-Jones potential is given by

$$\Phi = -\frac{A}{\rho^6} + \frac{B}{\rho^{12}} = 4\epsilon\left[-\left(\frac{\sigma}{\rho}\right)^6 + \left(\frac{\sigma}{\rho}\right)^{12}\right], \tag{1}$$

where ρ denotes the distance between two atoms, and A and B are the attractive and repulsive constants, respectively. Further, ϵ denotes a well depth and σ is the van der Waals diameter, and from which we may deduce that $A = 4\epsilon\sigma^6$ and

Author's personal copy

Table 1
Values of parameters used in the model.

Atom type	ϵ (kJ/mol)	σ (nm)	η (nm^{-2})
Q_0	5.000	0.4700	3.13×10^{-4}
Q_a	5.600	0.4700	3.13×10^{-4}
N_a	4.500	0.4700	3.13×10^{-4}
C_1	2.300	0.4700	$1.25 \times 10^{-3}/\ell$
Ag	0.036	0.3148	9.25×10^{-4}
Au	0.039	0.3293	8.45×10^{-4}

$B = 4\epsilon\sigma^{12}$. Moreover, the mixing rules $\sigma_{12} = (\sigma_1 + \sigma_2)/2$ and $\epsilon_{12} = \sqrt{\epsilon_1\epsilon_2}$ are utilised to determine the Lennard-Jones constants in a system with different atomic species.

Using a continuum approach, where atoms at discrete location on the molecule are averaged over its surface or its volume, the molecular interatomic energy can be obtained by calculating the integrals over the surface or the volume of each molecule, namely

$$E = \eta_1\eta_2 \int_{\Sigma_1}\int_{\Sigma_2} \left(-\frac{A}{\rho^6} + \frac{B}{\rho^{12}}\right) \mathrm{d}\Sigma_2\, \mathrm{d}\Sigma_1, \tag{2}$$

where η_1 and η_2 represent a mean surface density or a mean volume density of atoms on each molecule. From (2), the total axial force (in the z-direction) can be obtained as $F_z = -\partial E/\partial z$. For convenience, we may define the integral I_n as

$$I_n = \int_{\Sigma_1}\int_{\Sigma_2} \rho^{-2n}\, \mathrm{d}\Sigma_2\, \mathrm{d}\Sigma_1, \tag{3}$$

so that (2) can be written in the form

$$E = \eta_1\eta_2(-AI_3 + BI_6). \tag{4}$$

Here, our aim is to determine the critical dimension of the lipid nanotube which gives rise to the maximum suction energy upon the spherical molecule entering the nanotube. The suction energy is defined as the total work performed by the van der Waals interactions on a molecule entering a nanotube [18]. Mathematically, the suction energy W can be represented by

$$W = \int_{-\infty}^{\infty} F(z)\, \mathrm{d}z = -\int_{-\infty}^{\infty} \frac{\partial E}{\partial z}\, \mathrm{d}z = E(-\infty) - E(\infty). \tag{5}$$

In the case where there is no energy dissipation, the suction energy can be equated directly to the kinetic energy of the molecule.

A lipid nanotube is assumed to be composed of DPPC that are represented in the Martini force field by a head group, consisting of choline (Q_0) and phosphate (Q_a) groups, a glycerol group or an intermediate layer (N_a) and a tail group (C_1) [6]. Moreover, we assume that a spherical molecule considered here has the polarity of 3 (P_3). Further, Marrink et al. [6] employ the value of 0.64 nm^2 for the area per lipid, and there are two interaction sites for the head group and the intermediate layer, and eight interaction sites for the tail group. Consequently, the mean atomic surface density for the intermediate layer is given by $2/0.64$ nm^{-2}, and the mean atomic volume density for the head group is $2/(0.64\ell_h)$ nm^{-3} where ℓ_h is the thickness of the head group. The mean atomic volume density for the tail group can be obtained as $8/(0.64\ell_t)$ nm^{-3}, where the value of the tail length ℓ_t ranges from 1.5 nm to 2.0 nm. The schematic representation for a lipid nanotube and its structural dimension are depicted in Fig. 1, where $\ell_h = 0.4$ nm and $\ell_t = 1.6$ nm.

We choose to study two types of nanoparticles, namely silver (Ag) and gold (Au), to demonstrate the encapsulation behaviour inside a lipid nanotube. We note that we model these nanoparticles as perfect spheres. The Lennard-Jones parameters for both silver and gold are taken from Rappé et al. [19]. Since both silver and gold adopt a face-centred cubic (fcc) crystal structure, there are four atoms occupied in one unit cell. Assuming a cubic unit cell with a diagonal length on each face of $2d$, the volume of a unit cell is given by $V^\star = 2\sqrt{2}d^3$ Å^3 where d denotes the equilibrium spacing which can be obtained as $d = 2^{1/6}\sigma$. Consequently, the mean volume density η is given by $4/V^\star$. The Lennard-Jones parameters and the molecular densities used in this model are presented in Table 1.

3. Analytical evaluation for interaction energies

In this section, we evaluate the interaction energy for a spherical molecule (gold and silver nanoparticles) interacting with a lipid nanotube. The schematic model for this interaction is shown in Fig. 2. We note that the energy contribution from the sphere arises from all atoms, hence the spherical volume integral is utilised. For a lipid nanotube which is composed of a rolled-up lipid bilayer, we assume that there are six layers to be considered: two head groups, two intermediate layers and two tail groups. The intermediate layer is assumed to be a cylindrical surface whereas the head group and the tail group are assumed to be cylinders with thicknesses ℓ_h and ℓ_t, respectively. Thus, the total interaction energy of the system comprises:

(i) interaction energies between a spherical molecule and two head groups using cylindrical volume integral;

Author's personal copy

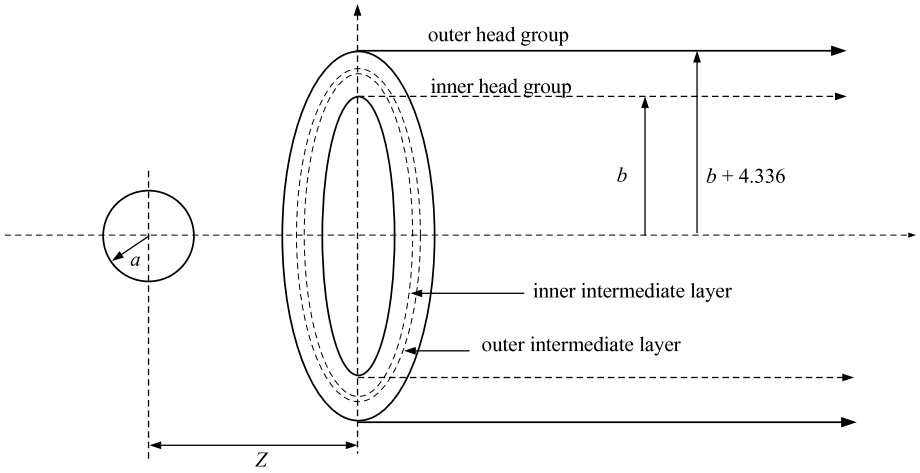

Fig. 2. Schematic model for a spherical molecule entering a lipid nanotube.

(ii) interaction energies between a spherical molecule and two intermediate layers using cylindrical surface integral;
(iii) interaction energies between a spherical molecule and two tail groups using cylindrical volume integral.

To obtain these interaction energies, we first consider the integral I_n ($n = 3, 6$) defined by (3) for the case of a spherical molecule of radius a centred at the origin interacting with a single atom located at $(0, 0, \delta)$. Following the work of the present authors [20], we express the volume integral I_3 and I_6 in terms of J_n as

$$I_3[J_n] = \frac{4}{3}\pi a^3 J_3, \tag{6}$$

$$I_6[J_n] = \frac{2}{45}\pi a^3 \left(30J_6 + 216a^2 J_7 + 432a^4 J_8 + 256a^6 J_9\right), \tag{7}$$

where $J_n = 1/(\delta^2 - a^2)^n$ and here n denotes a positive integer corresponding to the power of the polynomials appearing in I_3 and I_6 defined by (6) and (7), respectively.

In the following subsections, we determine the interaction energy between a spherical molecule and the surface of a cylindrical tube, and the interaction energy between a spherical molecule and the volume of a cylindrical tube of thickness ℓ.

3.1. Surface integral of a cylinder

In Cartesian rectangular coordinate system, the distance from the centre of a sphere $(0, 0, Z)$ to a typical point on a cylindrical surface of radius b is given by $\delta^2 = b^2 + (z - Z)^2$. Thus, we may deduce

$$J_n = \int_{-\pi}^{\pi}\int_0^L \frac{b}{[b^2 + (z - Z)^2 - a^2]^n}\,\mathrm{d}z\,\mathrm{d}\theta = 2\pi b\int_0^L \frac{1}{[b^2 + (z - Z)^2 - a^2]^n}\,\mathrm{d}z, \tag{8}$$

where L denotes the length of the tube. The distance between the centre of the sphere to the tube open end is defined by Z, which can be either positive (inside the tube) or negative (outside the tube). Next, we make the substitution $z - Z = \sqrt{b^2 - a^2}\tan\psi$ to obtain

$$J_n = \frac{2\pi b}{(b^2 - a^2)^{n-1/2}}\int_{-\tan^{-1}\left(Z/\sqrt{b^2-a^2}\right)}^{\tan^{-1}\left[(L-Z)/\sqrt{b^2-a^2}\right]} \cos^{2(n-1)}\psi\,\mathrm{d}\psi. \tag{9}$$

Noting that

$$\int \cos^{2(n-1)}\psi\,\mathrm{d}\psi = \frac{1}{2^{2(n-1)}}\left[\binom{2(n-1)}{(n-1)}\psi + \sum_{k=0}^{n-2}\binom{2(n-1)}{k}\frac{\sin[(2n-2k-2)\psi]}{(n-k-1)}\right], \tag{10}$$

where $\binom{n}{m}$ is the binomial coefficient. The formula (10) can be found in Gradshteyn and Ryzhik [21]. Finally, the interaction energy between a spherical molecule and the surface of a nanotube can be deduced using (4), (6), (7) and (9). Consequently, the suction energy (5) can be obtained by taking a limit of the interaction energy from $Z = -\infty$ to $Z = +\infty$.

Author's personal copy

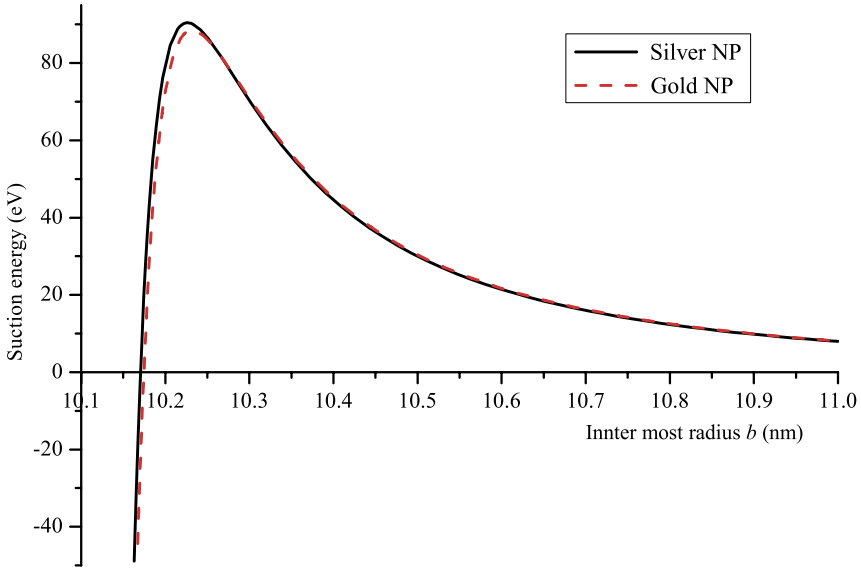

Fig. 3. Suction energy for silver and gold nanoparticles.

3.2. Volume integral of a cylinder with thickness ℓ

In the case of a sphere interacting with a nanotube of thickness ℓ, the volume integral J_n is given by

$$J_n = \int_{-\pi}^{\pi}\int_{b}^{b+\ell}\int_{0}^{L} \frac{r}{[r^2+(z-Z)^2-a^2]^n}\,\mathrm{d}z\,\mathrm{d}r\,\mathrm{d}\theta = 2\pi\int_{b}^{b+\ell}\int_{0}^{L} \frac{r}{[r^2+(z-Z)^2-a^2]^n}\,\mathrm{d}z\,\mathrm{d}r,$$

where ℓ is equal to the thickness of the tail group. On making the substitution $t = r^2+(z-Z)^2-a^2$, we may deduce

$$J_n = \frac{\pi}{(1-n)}\int_0^L \left(\frac{1}{[(b+\ell)^2+(z-Z)^2-a^2]^{n-1}} - \frac{1}{[b^2+(z-Z)^2-a^2]^{n-1}}\right)\mathrm{d}z. \tag{11}$$

Next, we substitute $z-Z = \sqrt{(b+\ell)^2-a^2}\tan\psi$ into the first term on the right hand side of (11) and $z-Z = \sqrt{b^2-a^2}\tan\psi$ to the second term. Thus, J_n becomes

$$J_n = \frac{\pi}{(1-n)}\left[\frac{1}{[(b+\ell)^2-a^2]^{n-3/2}}\int_{-\tan^{-1}(Z/\sqrt{(b+\ell)^2-a^2})}^{\tan^{-1}[(L-Z)/\sqrt{(b+\ell)^2-a^2}]}\cos^{2(n-2)}\psi\,\mathrm{d}\psi - \frac{1}{(b^2-a^2)^{n-3/2}}\int_{-\tan^{-1}(Z/\sqrt{b^2-a^2})}^{\tan^{-1}[(L-Z)/\sqrt{b^2-a^2}]}\cos^{2(n-2)}\psi\,\mathrm{d}\psi\right]. \tag{12}$$

The analytical expression for J_n can be obtained by using (10). Finally, the interaction energy between a spherical molecule and the volume of a nanotube can be obtained by using (4), (6), (7) and (12). As a result, we can find the suction energy (5) by taking a limit of the interaction energy from $Z=-\infty$ to $Z=+\infty$.

4. Numerical results and discussion

In this section, we provide numerical results for the interaction energy between a spherical molecule of radius a and a lipid nanotube of the inner-most radius b. The radii of the nanoparticles are assumed to be 10 nm and the length of the tube is taken to be 100 nm. The Lennard-Jones parameters and the molecular densities are as given in Table 1. Fig. 3 shows the suction energy for silver and gold nanoparticles as a function of the radius of a lipid nanotube. We find that the suction energy for the silver nanoparticle is positive when the inner-most radius of the tube $b_0 \geq 10.171$ nm, and the maximum suction energy occurs at $b_{max} = 10.227$ nm. For the gold nanoparticle, we obtain $b_0 \geq 10.177$ nm and $b_{max} = 10.232$ nm. We comment that b_0 represents the minimum size of the inner-most radius of the nanotube which will accept the nanoparticle from rest, and that b_{max} is the critical size which will optimise the interaction between the nanotube and the nanoparticle. We note that the length of the lipid nanotube only has a minor effect on b_0 and b_{max}; it will only affect the magnitude of the suction energy.

Author's personal copy

This method can also be applied to study the suction of a protein molecule into a lipid nanotube. Here, protein trypsin is chosen to demonstrate such behaviour. Trypsin is a globular protein with a hydrodynamic diameter of 3.8 nm and the Lennard-Jones parameters of trypsin can be found in Ref. [20]. By using the same method described in this paper, we obtain a similar suction energy profile to those of gold and silver nanoparticles. Since the radius of trypsin is only 1.9 nm, we find that $b_0 \geq 2.017$ nm and $b_{max} = 2.052$ nm.

In general, this model can be used to determine the van der Waals potential energy for any dense spheres interacting with a lipid nanotube. Through this model, one can predict the minimum size of the lipid nanotube that will allow the entrance of a dense spherical molecule and also the critical size of the tube that will maximise their interaction leading to a stable system. For different types of spherical molecules, even though we expect similar trend for the energy profiles, the magnitude of the potential energy and the values of b_0 and b_{max} will be different, as they depend on the atomic component and the size of the encapsulated molecules. Furthermore, we note that as the radius of the nanotube becomes larger we expect the same behaviour seen in Ref. [22] that the encapsulated molecule will move closer to the side-wall of the nanotube to minimise the interaction energy.

Finally, we comment that the main contribution of this paper is the derivation of the analytical expressions for the interaction energy between a dense spherical molecule and a lipid nanotube. As they are given as a function of the radius of the sphere, the radius and the length of the nanotube, the model developed here can be extended to investigate other scenarios which may involve the encapsulation of other spherical molecules (e.g. drugs and proteins) inside a lipid nanotube. Such studies would contribute to the development of a lipid nanotube as a carrier for drug and gene delivery.

Acknowledgements

The authors acknowledge the financial support from the University of Wollongong's Internationalisation Linkage Grant Scheme. DB gratefully thanks the Thailand Research Fund (TRG5680072).

References

[1] N. Nishiyama, Nanomedicine: nanocarriers shape up for long life, Nat. Nanotechnol. 2 (2007) 203–204.
[2] Y. Zhou, T. Shimizu, Lipid nanotubes: a unique template to create diverse one-dimensional nanostructures, Chem. Mater. 20 (2008) 625–633.
[3] T. Shimizu, Self-assembled lipid nanotube hosts: the dimension control for encapsulation of nanometer-scale guest substances, J. Polym. Sci. A 44 (2006) 5137–5152.
[4] Y. Zhou, Lipid nanotubes: formation, templating nanostructures and drug carriers, Cri. Rev. Solid State 33 (2008) 183–196.
[5] R. DeVane, A. Jusufi, W. Shinoda, C.-C. Chiu, S. Nielsen, P.B. Moore, M.L. Klein, Parametrization and application of a coarse grained force field for benzene/fullerene interactions with lipids, J. Phys. Chem. B 114 (2010) 16364–16372.
[6] S.J. Marrink, H.J. Risselada, S. Yefimov, D.P. Tieleman, A.H. de Vries, The MARTINI force field: coarse grained model for biomolecular simulations, J. Phys. Chem. B 111 (2007) 7812–7824.
[7] S.J. Marrink, A.H. de Vries, A.E. Mark, Coarse grained model for semiquantitative lipid simulations, J. Phys. Chem. B 108 (2004) 750–760.
[8] J.C. Shelley, M.Y. Shelley, R.C. Reeder, S. Bandyopadhyay, P.B. Moore, M.L. Klein, Simulations of phospholipids using a coarse grain model, J. Phys. Chem. B 105 (2001) 9785–9792.
[9] W. Shinoda, R. DeVane, M.L. Klein, Zwitterionic lipid assemblies: molecular dynamics studies of monolayers, bilayers, and vesicles using a new coarse grain force field, J. Phys. Chem. B 114 (2010) 6836–6849.
[10] E.J. Wallace, M.S.P. Sansom, Carbon nanotube/detergent interactions via coarse-grained molecular dynamics, Nano Lett. 7 (2007) 1923–1928.
[11] J. Wong-Ekkabut, S. Baoukina, W. Triampo, I.M. Tang, D.P. Tieleman, L. Monticelli, Computer simulation study of fullerene translocation through lipid membranes, Nat. Nanotechnol. 3 (2008) 363–368.
[12] D. Baowan, B.J. Cox, J.M. Hill, Instability of C_{60} fullerene interacting with lipid bilayer, J. Mol. Mod. 18 (2012) 549–557.
[13] B. Chithrani, A. Ghazani, W. Chan, Determining the size and shape dependence of gold nanoparticle uptake into mammalian cells, Nano Lett. 6 (2006) 662–668.
[14] Q. Pu, Y. Leng, X. Zhao, P. Cummings, Molecular simulations of stretching gold nanowires in solvents, Nanotechnology 18 (2007) 424007.
[15] M. Ahamed, M.S. Alsalhi, M.K. Siddiqui, Silver nanoparticle applications and human health, Clin. Chim. Acta 411 (2010) 1841–1848.
[16] K.M.M.A. El-Noura, A. Eftaihab, A. Al-Warthanb, R.A.A. Ammarb, Synthesis and applications of silver nanoparticles, Arab. J. Chem. 3 (2010) 135–140.
[17] D. Baowan, H. Peuschel, A. Kraegeloh, V. Helms, Energetics of liposomes encapsulating silica nanoparticles, J. Mol. Mod. 19 (2013).
[18] B.J. Cox, N. Thamwattana, J.M. Hill, Mechanics of atoms and fullerenes in single-walled carbon nanotubes, I. Acceptance and suction energies, Proc. R. Soc. A 463 (2007) 461–476.
[19] A.K. Rappé, C.J. Casewit, K.S. Colwell, W.A. Goddard III, W.M. Skiff, UFF, a full periodic table force field for molecular mechanics and molecular dynamics simulations, J. Am. Chem. Soc. 114 (1992).
[20] D. Baowan, N. Thamwattana, Modelling selective separation of trypsin and lysozyme using mesoporous silica, Macro. Meso. Meterials 176 (2013) 209–214.
[21] I.S. Gradshteyn, I.M. Ryzhik, Table of Integrals, Series, and Products, seventh ed., Academic Press, 2007.
[22] B.J. Cox, N. Thamwattana, J.M. Hill, Mechanics of atoms and fullerenes in single-walled carbon nanotubes, II. Oscillatory behaviour, Proc. R. Soc. A 463 (2007) 477–494.

J Math Chem (2015) 53:29–40
DOI 10.1007/s10910-014-0408-z

ORIGINAL PAPER

Quantitative study of BSA coating silica nanoparticle

Duangkamon Baowan · Volkhard Helms

Received: 15 July 2014 / Accepted: 13 September 2014 / Published online: 27 September 2014
© Springer International Publishing Switzerland 2014

Abstract The loading of biomolecules on nanoparticles might be thought of as a first step to design a cargo in drug delivery system. Here, we study a quantity of bovine serum albumin (BSA) surrounding the silica nanoparticle. The silica nanoparticle is modeled as a perfect sphere whereas the BSA is represented by an ellipsoid. On utilizing a continuous approximation, the electrostatic and van der Waals interactions can be analytically expressed. Further, a number of BSA molecules coating on the nanoparticles of various sizes can be simply determined as a function of the protein ring radius. Our finding is in a good agreement found in experiment and this can be a guide to evaluate the number of protein on other type of spherical nanoparticles.

Keywords Bovine serum albumin · Silica nanoparticle · Lennard-Jones function · Coulombic function

1 Introduction

The integration of nanoparticles with biomolecules may yield novel hybrid nanobiomaterials of combined properties and functions arising from the unique physical and chemical properties of nanoparticles and the unique recognition by cell of biomaterials. There is a growing knowledge that the fundamental interactions of nanoscale

D. Baowan (✉)
Department of Mathematics, Faculty of Science, Mahidol University,
Rama VI, Bangkok 10400, Thailand
e-mail: duangkamon.bao@mahidol.ac.th

V. Helms
Center for Bioinformatics, Saarland University, Campus E2 1, 66123 Saarbrücken, Germany

objects with living substance play a major role in nanomedicine, as well as in terms of nanosafety issue [1]. For this reason the study of the nanoparticles coated by protein as a protein corona might be thought of as a first step to create drug or gene delivery systems.

In biomedical field, silica nanoparticles may serve as a delivery system for drugs and genes [2,3]. For example, DNA can be functionalized on the surface of silica nanoparticles and is transported into animal tissues [4–9]. Moreover, these nanoparticles may bind to drugs and serve as a cargo to deliver such molecules to the targeted cells [3,10–12]. In particular, Schübbe et al. [13] investigated the location of SiO_2 nanoparticles of 32 and 83 nm in diameters in Caco-2 cells as a model of human intestinal cells, and they found that silica of both sizes can enter into the cytoplasm. With increasing incubation time, the particles move towards the nucleus of the cells.

Bovine serum albumin (BSA) has been widely used as a protein model in many applications both in industry and academic research [14]. This protein is essential for the transportation of hormones and fatty acids in mammals. BSA has an isoelectric point at pH 4.75, and carries a negative net charge at pH 7. Wright and Thompson [15] proposed a prolate ellipsoid model for BSA with the dimensions of $2a = 140.4 \pm 4.9$ Å and $2b = 2c = 41.6 \pm 3.6$ Å. According to structure determination by Carter et al. [14,16] using X-ray diffraction, the three-dimensional structure of BSA is proposed as a heart-shaped comprising three homologous domains. Röcker et al. [17] studied a number of BSA coating FePt and CdSe/Zns nanoparticles, and found a thickness of the protein corona of approximately 3.3 nm. In case of the interaction between BSA and silica nanoparticles, Su et al. [18] observed by neutron reflection that a uniform layer of the protein adsorbed at the hydrophilic silica-water interface. They suggested that the layer thickness is always <4 nm.

The mechanics of silica nanoparticle coated with a layer of BSA, in terms of energy calculation, may be determined using a continuous approach. Here one assumes that discrete atomic arrangements can be replaced by a uniform atomic distribution, so that the total interaction energy between two molecules can be evaluated using an integral technique. In the case of interaction energy between nano-structures, Girifalco et al. [19,20] applied the continuous approach to analytically derive the potential energies for various arrangements of a carbon nanotube and a C_{60} fullerene. This continuous approximation can also be used to determine the interaction energy between an organic molecule, C_{60} fullerene, and a biological structure, lipid bilayer, as proposed by Baowan et al. [21] where they studied the location of fullerene penetrating to the DPPC lipid bilayers. Recently, the authors utilized the same method to study the encapsulation of silica nanoparticles in liposomes [22].

By using techniques from applied mathematics, this paper aims at determining a number of protein molecules coating silica nanoparticles of different sizes. We account for electrostatic interactions by a Coulombic term and by the Born equation for the solvation free energy, where they are detailed in Sect. 2. Further, we utilize the Lennard-Jones potential function for the van der Waals interaction. The model formulation for the BSA surrounding the silica nanoparticles is presented in Sect. 3 followed by the numerical results. Finally, the summary is presented in Sect. 5.

2 Method

Here, we determine the optimal number of proteins in a monolayer coating a sliica nanoparticle. Instead of using complicated force fields, we employ the continuous approach for modeling the total non-bonded energy. Both van der Waals and electrostatic interactions are taken into account.

The standard 6–12 Lennard-Jones function is given by

$$\Phi = -\frac{A}{\rho^6} + \frac{B}{\rho^{12}} = 4\epsilon\left[-\left(\frac{\sigma}{\rho}\right)^6 + \left(\frac{\sigma}{\rho}\right)^{12}\right],$$

where ρ denotes the distance between two typical points, and A and B are attractive and repulsive Lennard-Jones constants, respectively.

The electrostatic energy for molecules carrying partial charges can be modeled using the sum of Coulombic function and Born equation to account for the solvation energy [23] which is given by

$$U = \frac{q_i q_j}{4\pi\epsilon_0\epsilon_r}\frac{1}{\rho} - \frac{1}{8\pi}\left(\frac{1}{\epsilon_i} - \frac{1}{\epsilon_r}\right)\frac{q_i q_j}{f_{GB}},$$

where ρ denotes the distance between two typical charge centers, q_i and q_j are partial point charges, ϵ_0 denotes the vacuum permittivity of $8.85 \times 10^{-12}\,\mathrm{CV^{-1}m^{-1}}$, and ϵ_i and ϵ_r are relative dielectric constants. The generalized Born equation (f_{BG}) is given by $f_{GB} = \sqrt{\rho^2 + a^2 e^{-\rho^2/(4a^2)}}$ where a is the van der Waals radius of a charged particle, and for $\rho \gg a$ we may approximate $f_{GB} = \rho$. Therefore, the electrostatic term becomes

$$U = \frac{q_i q_j}{4\pi}\left[\frac{1}{\epsilon_r\epsilon_0} - \frac{1}{2}\left(1 - \frac{1}{\epsilon_r}\right)\right]\frac{1}{\rho},$$

where we take $\epsilon_i = 1$.

Using the continuous approach, where the atoms at discrete locations of the molecule are averaged over a surface or a volume, the molecular interatomic energy is obtained by calculating integrals over the surface or the volume of each molecule, which is given by

$$E = \eta_1\eta_2\int_{S_1}\int_{S_2}\left\{\left(-\frac{A}{\rho^6} + \frac{B}{\rho^{12}}\right) + \frac{q_i q_j}{4\pi}\left[\frac{1}{\epsilon_r\epsilon_0} - \frac{1}{2}\left(1 - \frac{1}{\epsilon_r}\right)\right]\frac{1}{\rho}\right\} dS_2 dS_1,$$

where η_1 and η_2 represent the average surface or the average volume density of atoms on each molecule. For convenience, we define

$$I_n = \int_{S_2}\int_{S_1}\rho^{-2n} dS_1 dS_2, \tag{1}$$

where $n = 1/2$, 3 and 6 correspond to the degree of ρ that appears in the above energy equation.

Table 1 Lennard-Jones and Coulombic parameters for silica nanoparticle used in this model

Atom type	ϵ (kJ/mol)	σ (nm)	q (C)	Dangling atom density (nm^{-2})
Si	1.297	0.4295	$+0.3\|e\|$	1.0
O	0.628	0.3500	$-0.3\|e\|$	1.0

Table 2 Lennard-Jones parameters for BSA used in this model

Atom type	ϵ (kJ/mol)	σ (nm)	Number of atoms in one molecule
C	0.0951	0.30275	3,072
H	0.0512	0.28464	4,828
N	0.0774	0.32626	816
O	0.0957	0.30332	928
S	0.3440	0.35903	40

The Lennard-Jones and Coulombic constants for silica nanoparticle are taken from the work of Cruz-Chu et al. [24] and are listed in Table 1. Here, SiO_2 is modeled as a perfect spherical molecule where the Si atom is located at the center and the bond length between Si and O is 0.161 nm. Then the average atomic surface density of silica may be obtained as $3/[4\pi(0.161)^2] = 9.325\,\mathrm{nm}^{-2}$, where 3 is the number of atoms in a molecule. Similarly, the average atomic volume density of silica is given by $3/[(4/3)\pi(0.161)^3] = 171.61\,\mathrm{nm}^{-3}$. Further, it is assumed to be comprised at the inside of small overall neutral SiO_2 beads whereas the outer surface of the solvated nanoparticle is partially covered by silanol (–SiOH) groups [24,25]. Following the work of Cruz-Chu et al. [24], the density of the dangling atoms of silicon and oxygen are approximately $1\,\mathrm{nm}^{-2}$. Therefore, to guarantee the neutral charge of the silica nanoparticle, the partial charges for the silicon atoms and hydroxyl groups are taken to be $+0.3|e|$ and $-0.3|e|$, respectively.

We model the BSA protein as an ellipsoid with dimensions of $14 \times 4 \times 4\,\mathrm{nm}$ [15]. This gives a volume of $117.29\,\mathrm{mn}^3$ for one protein molecule. The BSA molecule comprises of 9,684 atoms in total, and therefore the average atomic volume density of the BSA is 82.57 atoms per cubic nanometer. The electrostatic interactions of proteins are mostly due to polar and charged amino acids on the surface. According to the assumed ellipsoidal shape, the surface area of such a BSA molecule is approximately $142.31\,\mathrm{nm}^2$, then the average atomic surface density of the BSA is $68.05\,\mathrm{nm}^{-2}$. Here, we vary the charge of the BSA to represent the pH or ion concentration in an environment. The Lennard-Jones parameters for the atomic components of BSA are taken from the work of Mayo et al. [26], and are presented in Table 2. Mixing rule is employed to study the interaction between two atomic types.

3 Model formulation

According to Röcker et al. [17] and Su et al. [18], BSA forms a monolayer when surrounding nanoparticles. Here, we assume that the protein forms layer of ℓ nm thickness surrounding a spherical nanoparticle of radius a, where ℓ ranges from 4 to 14 nm

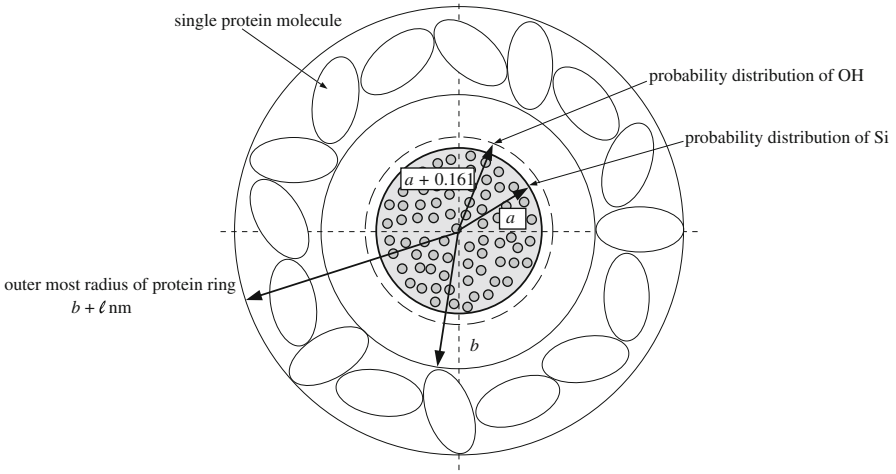

Fig. 1 Model formation for silica nanoparticle coated by BSA where b is the inner most ring radius and ℓ is the thickness of the ring which ranges from 4 to 14 nm

corresponding to the dimensions of a BSA molecule. The silica nanoparticle is assumed to be centered at the origin as shown in Fig. 1. Therefore, the total energy of the system consists of

1. The van der Waals energy between the volume of the spherical protein ring and the volume of the spherical nanoparticle.
2. The electrostatic energy between the surface of the protein ring and the surface of the nanoparticle arising from the silica atoms and hydroxyl groups.

The volume of the protein ring around the nanoparticle V_{layer} is given by

$$V_{layer} = \frac{4}{3}\pi\left[(b+\ell)^3 - b^3\right],$$

where b denotes an inner most radius of the protein ring which needs to be determined as a solution of the problem. It can be shown that a volume of an ellipsoid of dimensions $2a \times 2b \times 2b$ is approximately two thirds of a volume of a cylinder with the height of $2a$ and the diameter of $2b$. Accordingly, the amount of the protein molecule in the spherical protein ring is approximately $2V_{layer}/3$. Therefore, the number of BSA molecules coating the silica nanoparticle can be determined by

$$N_p = \frac{2V_{layer}}{3V_p} = \frac{2[(b+\ell)^3 - b^3]}{3(2)(2)(7)} = \frac{(b+\ell)^3 - b^3}{42}, \tag{2}$$

where V_p is the volume of one BSA molecule.

The schematic models for the van der Waals and the electrostatic interactions are depicted in Fig. 2. We firstly determine the molecular interaction between a surface or a volume of a sphere and a single atom as shown in Fig. 2a. Then, the single atom is assumed to be located on the other spherical surface, and either volume or

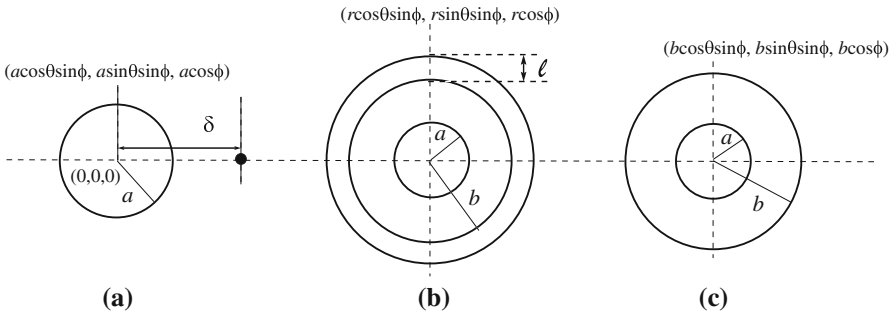

Fig. 2 Schematic structures for **a** a sphere interacting with a single atom, **b** concentric spheres for the outer volume integral, and **c** concentric spheres for the outer surface integral

surface integral is applied to determine the total energy of the system. Mathematical derivations for the van der Waals and the electrostatic interactions using in this model are presented in Sects. 3.1 and 3.2, respectively.

3.1 Van der Waals interaction

We begin by considering the integral I_n defined by (1) for $n = 3, 6$ and for a spherical molecule of radius a centered at the origin and a point located at $(0, 0, \delta)$, as shown in Fig. 2a. The distance from a typical element of the sphere to the atom is given by $\rho^2 = (r\cos\theta\sin\phi)^2 + (r\sin\theta\sin\phi)^2 + (r\cos\phi - \delta)^2$, $r \in [0, a]$. Following the work by Baowan and Thamwattana [27], it is convenient to express the volume integral I_3 and I_6 in terms of J_n which is defined by $J_n = 1/(\delta^2 - a^2)^n$ where n is a positive integer corresponding to the power of the polynomials appearing in I_3 and I_6 defined by (3) and (4), respectively. This gives

$$I_3[J_n] = \frac{4}{3}\pi a^3 J_3, \tag{3}$$

$$I_6[J_n] = \frac{2}{45}\pi a^3 \left(30J_6 + 216a^2 J_7 + 432a^4 J_8 + 256a^6 J_9\right). \tag{4}$$

Next, we need to evaluate the volume integral for the outer spherical ring where the schematic model is shown in Fig. 2b. The distance δ from the center of the first sphere to a typical point on the spherical ring is given by $\delta = r$ and, therefore we may deduce

$$\begin{aligned} L_n^{LJ} &= \int_V J_n dS = \int_{-\pi}^{\pi}\int_b^{b+\ell}\int_0^{\pi} \frac{r^2\sin\phi}{(r^2-a^2)^n} d\phi dr d\theta \\ &= \frac{4\pi(-1)^n}{a^{2n-3}} \int_{\sin^{-1}(b/a)}^{\sin^{-1}[(b+\ell)/a]} \left[\frac{1}{\cos^{2n-1}(t)} - \frac{1}{\cos^{2n-3}(t)}\right] dt, \end{aligned} \tag{5}$$

where ℓ is the thickness of the ring, and for any given value of n, an analytic expression of L_n^{LJ} can be obtained. The total van der Waals interaction between the sphere and the

spherical ring of thickness ℓ can be obtained by substituting L_n^{LJ} defined by (5) into I_3 and I_6 defined by (3) and (4), respectively. Therefore, the van der Waals interaction between the spherical molecule of radius a and the spherical ring of thickness ℓ is given by

$$P_{1-2} = \eta_1\eta_2\left\{-A_{1-2}\left(\frac{4}{3}\pi a^3 L_3^{LJ}\right) + B_{1-2}\left[\frac{2}{45}\pi a^3\left(30L_6^{LJ} + 216a^2L_7^{LJ} + 432a^4L_8^{LJ} + 256a^6L_9^{LJ}\right)\right]\right\}, \tag{6}$$

where η_1 and η_2 represent the average atomic volume densities of the sphere and the protein ring, respectively, and A_{1-2} and B_{1-2} are the Lennard-Jones attractive and repulsive constants, respectively.

Hence, the total van der Waals interaction between the spherical silica nanoparticle and the ring of the BSA with thickness ℓ is given by

$$\begin{aligned} E_{vdW} = {} & \left(\frac{1}{3}\right)\left[\left(\frac{3072}{9684}\right)P_{Si-C} + \left(\frac{4828}{9684}\right)P_{Si-H} + \left(\frac{816}{9684}\right)P_{Si-N} \right. \\ & \left. + \left(\frac{928}{9684}\right)P_{Si-O} + \left(\frac{40}{9684}\right)P_{Si-S}\right] \\ & + \left(\frac{2}{3}\right)\left[\left(\frac{3072}{9684}\right)P_{O-C} + \left(\frac{4828}{9684}\right)P_{O-H} + \left(\frac{816}{9684}\right)P_{O-N} \right. \\ & \left. + \left(\frac{928}{9684}\right)P_{O-O} + \left(\frac{40}{9684}\right)P_{O-S}\right], \end{aligned} \tag{7}$$

where P_{1-2} is defined by (6). The rational coefficients come from the proportional content of 1/3 silicon and 2/3 oxygen atoms in the silica nanoparticle. By the same consideration the atomic proportions for the BSA can be obtained, this yields the value of 9684 in the denominator.

3.2 Electrostatic interaction

For this we consider the integral I_n defined in Eq. (1) with $n = 1/2$. In the case of a spherical surface interacting with a single atom, as depicted in Fig. 2a, we may deduce

$$\begin{aligned} I_{1/2} &= \int_s \frac{1}{\rho}dS = \int_{-\pi}^{\pi}\int_0^{\pi} \frac{a^2\sin\phi}{(a^2+\delta^2-2a\delta\cos\phi)^{1/2}}d\phi d\theta \\ &= \frac{\pi a}{\delta}\int_{(\delta-a)^2}^{(\delta+a)^2}\frac{1}{\sqrt{t}}dt \\ &= 4\pi a^2\frac{1}{\delta}, \end{aligned} \tag{8}$$

where δ is the distance from the center of the sphere to the atom.

Next we aim to integrate $1/\delta$ over another concentric spherical structure. As shown in Fig. 2c, we have $\delta = b$, and we may deduce

$$L^{Q}_{1/2}(a,b) = 4\pi a^2 \int_S \frac{1}{\delta} dS = 4\pi a^2 \int_{-\pi}^{\pi}\int_0^{\pi} \frac{b^2 \sin\phi}{b} d\phi d\theta = 16\pi^2 a^2 b. \quad (9)$$

Then the electrostatic interaction between two concentric spheres is given by

$$Q_{1-2} = 4\pi \eta_1^* \eta_2^* q_1 q_2 \left[\frac{1}{\epsilon_r \epsilon_0} - \frac{1}{2}\left(1 - \frac{1}{\epsilon_r}\right)\right] a^2 b, \quad (10)$$

where in this case η_1^* and η_2^* are the average atomic surface densities of the nanoparticle and the protein molecule, respectively. Hence, the total electrostatic interaction between the ring of BSA and the surface of the silica nanoparticle arising from the two layers of silica atoms and hydroxyl groups can be deduced

$$E_{elec} = 4\pi \eta_1^* \eta_2^* q_2 \left[\frac{1}{\epsilon_r \epsilon_0} - \frac{1}{2}\left(1 - \frac{1}{\epsilon_r}\right)\right] \left[0.3|e|a^2 b - 0.3|e|(a + 0.161)^2 b\right], \quad (11)$$

where q_2 denotes the total charge of the BSA. Here, the probability distribution of silica atoms is assumed to be on the spherical surface of radius a and the probability distribution of hydroxyl group is assumed to be on the spherical surface of radius $a + 0.161$ nm.

4 Numerical results and discussion

Due to the unknown BSA charge q_2, here we assume three possible negative charge values which are $-0.1|e|$, $-0.3|e|$ and $-0.5|e|$. This is from the fact that BSA carries a negative net charge at pH 7. The dielectric constant ϵ_r is taken to be 80 as the relative permittivity of water. We note that the value of ϵ_r does not effect the physical behaviour of the system [22]. The electrostatic energy profiles for the three negative charge values are shown in Fig. 3. We found that increasing the magnitude of the charge increases the magnitude of the electrostatic energy in the system. The positive total energy comes from the repulsion between the assumed negative charge of the protein and the negative charge of the hydroxy group. Further, we found that the value of the electrostatic energy has three orders of magnitude lower than the value of the van der Waals energy. Therefore, only the van der Waals interaction is needed in order to determine the optimum ring radius b.

The summation of the van der Waals and the electrostatic energies given in (7) and (11) gives rise to the total energy of the system. Figure 4 shows an energy profile for the specific value of the silica nanoparticle radius $a = 15$ nm at the isoelectric point. We obtained the optimum radius of the inner ring at $b = 15.37$ nm. The other sizes of silica nanoparticles give the same energy behaviors, and they are not shown here.

A number of BSA molecules surrounding the silica nanoparticle can be calculated by the relation given by (2). The radius of the protein ring b is determined at the

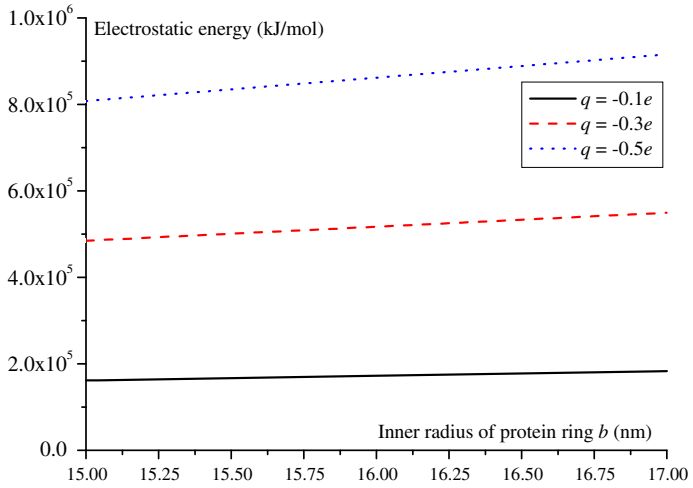

Fig. 3 Electrostatic energy for three different negative charge values on BSA for silica nanoparticle of radius 15 nm coated by BSA

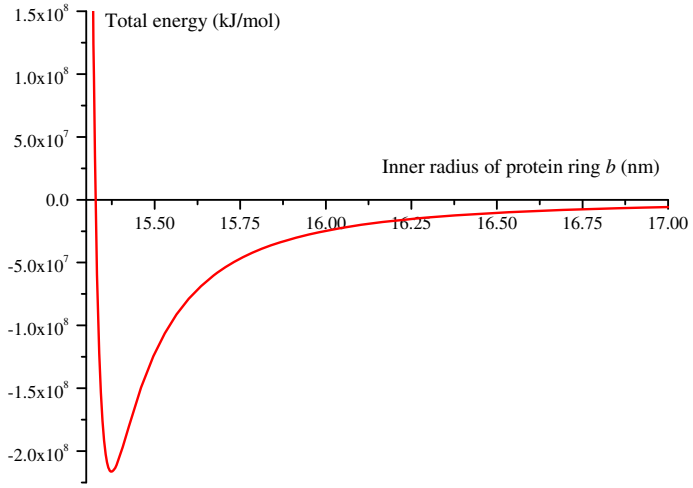

Fig. 4 Total energy at an isoelectric point of silica nanoparticle of radius 15 nm coated by BSA

equilibrium position, and their values for five different sizes of silica nanoparticles are given in Table 3. We assume three values for the ring thickness ℓ arising from the maximum, average and minimum dimensions of a BSA molecule, which are 14, 7.33 and 4 nm, respectively. We found that the number of protein molecules coating the nanoparticles is independent of the charge values on BSA. Moreover when ℓ is assumed to be 4 nm, our result for the case of $a = 5.6$ nm is in a good agreement with the number given by Röcker et al. [17] where we predict that there are 21 BSA molecules surrounding the nanoparticle and they obtained 23 molecules coating the nanoparticle. Further, 4 nm is also represented the protein thickness surrounding the silica nanoparticle as proposed by Su et al. [18].

Table 3 Numerical results for the inner most radius b of BSA and a number of proteins N_p coating silica nanoparticle

a (nm)	Inner most radius b (nm)	Number of proteins N_p		
		$\ell = 14$ nm	$\ell = 7.33$ nm	$\ell = 4$ nm
5.6	5.974	187	54	21
10	10.374	331	119	57
15	15.374	560	235	130
20	20.374	866	406	244
25	25.374	1,259	638	409

The main result of this paper is the derivation of an analytical expression for the total energy of the system as a function of a spherical core radius. The silica nanoparticle is introduced here as a model particle to illustrate the physical properties such as size and charge. Once the particle type is replaced by another material, only the parameters and constants need to be changed, but the mathematical expressions derived here remain the same. Similarly, the type of a protein molecule can be changed and only the proportion of atomic species are needed to be adjusted. Furthermore, the calculation of a number of protein molecules loading on the nanoparticle can be easily modified utilizing different geometries of the protein molecules.

5 Summary

A quantitative determination of BSA monolayer coating on a silica nanoparticle surface is studied here, which might be thought of as a delivery process of biomolecules on the nanoparticle as a targeted drug cargo. Both van der Waals and electrostatic interaction energies are taken into account utilizing the Lennard-Jones potential and the Coulombic potential including Born equation. The continuous approach, where the atoms in a molecule are assumed to be uniformly distributed over a surface or a volume of the molecule, is employed to determine the total energy of the system. Then the surface and the volume integral techniques are utilized to analytically express the model calculations. In this study, we assume that the silica nanoparticle can be modeled as a perfect sphere whereas the BSA can be represented by an ellipsoid.

Due to an unknown charge on the protein molecule, we assume three possible negative charge values which are $-0.1|e|$, $-0.3|e|$ and $-0.5|e|$. The total interaction energy for the silica nanoparticle coated by BSA is obtained as a function of the nanoparticle size and the charge of the protein. The solution of the problem is the inner most radius of the protein ring which will be used to determine the quantity of the protein surrounding the nanoparticle. Three values of ring thickness ℓ are assumed. Further, we found that the number of protein molecules on the silica nanoparticle cannot be explained by charge effects and Coulomb interaction, it depends on the van der Waals interaction alone. Moreover, the results obtained here are comparable with the ones obtained in experiments. Our work thus could be viewed as a first step toward designing cargo to load the biomolecules on the organic nanoparticle.

Acknowledgments This work is supported by a postdoctoral fellowship to D.B. by Alexander von Humboldt Foundation. D.B. gratefully thanks the Thailand Research Fund (MRG5680072). The authors also gratefully thanks H. Peuschel and A. Kraegeloh from Nano Cell Interactions Group, INM-Leibniz Institute for New Materials, Saarbrücken, Germany for many helpful discussion.

References

1. I. Lynch, T. Cedervall, M. Lundqvist, C. Cabaleiro-Lago, S. Linse, K.A. Dawson, The nanoparticle–protein complex as a biological entity; a complex fluids and surface science challenge for the 21st century. Adv. Colloid Interface Sci. **134–135**, 167–174 (2007)
2. M.J. Heller, DNA microarray technology: devices, systems, and applications. Annu. Rev. Biomed. Eng. **4**, 129–153 (2002)
3. I.I. Slowing, J.L. Vivero-Escoto, C.-W. Wu, V.S.-Y. Lin, Mesoporous silicananoparticles as controlled release drug delivery and gene transfection carriers. Adv. Drug Deliv. Rev. **60**, 1278–1288 (2008)
4. C. Kneuer, M. Sameti, U. Bakowsky, T. Schiestel, H. Schirra, H. Schmidt, C.-M. Lehr, A nonviral DNA delivery system based on surface modified silica-nanoparticles can efficiently transfect cells in vitro. Bioconjug. Chem. **11**, 926–932 (2000)
5. D. Luo, E. Han, N. Belcheva, W.M. Saltzman, A self-assembled, modular DNA delivery system mediated by silicananoparticles. J. Control. Release **95**, 333–341 (2004)
6. D.R. Radu, C.-Y. Lai, K. Jeftinija, E.W. Rowe, S. Jeftinija, V.S.-Y. Lin, A polyamidoamine dendrimer-capped mesoporous silica nanosphere-based gene transfection reagent. J. Am. Chem. Soc. **126**, 1321–13217 (2004)
7. I. Roy, T.Y. Ohulchanskyy, D.J. Bharali, H.E. Pudavar, R.A. Mistretta, N. Kaur, P.N. Prasad, Optical tracking of organically modified silica nanoparticles as DNA carriers: a nonviral, nanomedicine approach for gene delivery. Proc. Natl. Acad. Sci. USA **102**, 279–284 (2005)
8. D.J. Bharali, I. Klejbor, E.K. Stachowiak, P. Dutta, I. Roy, N. Kaur, E.J. Bergey, P.N. Prasad, M.K. Stachowiak, Organically modified silica nanoparticles: a nonviral vector for in vivo gene delivery and expression in the brain. Proc. Natl. Acad. Sci. USA **102**, 11539–11544 (2005)
9. T. Xia, M. Kovochich, M. Liong, H. Meng, S. Kabehie, S. George, J.I. Zink, A.E. Nel, Polyethyleneimine coating enhances the cellular uptake of mesoporous silica nanoparticles and allows safe delivery of siRNA and DNA constructs. ACS Nano **3**, 3273–3286 (2009)
10. I.I. Slowing, B.G. Trewyn, S. Giri, V.S.-Y. Lin, Mesoporous silica nanoparticles for drug delivery and biosensing applications. Adv. Funct. Mater. **17**, 1225–1236 (2007)
11. J.-F. Chen, H.-M. Ding, J.-X. Wang, L. Shao, Preparation and characterization of porous hollow silicananoparticles for drug delivery application. Biomaterials **25**, 723–727 (2004)
12. J.L. Vivero-Escoto, I.I. Slowing, B.G. Trewyn, V.S.-Y. Lin, Mesoporous silica nanoparticles for intracellular controlled drug delivery. Small **6**, 1952–1967 (2010)
13. S. Schübbe, C. Schumann, C. Cavelius, M. Koch, T. Mueller, A. Kraegeloh, Size-dependent localization and quantitative evaluation of the intracellular migration of silica nanoparticles in Caco-2 cells. Chem. Mater. **24**, 914–923 (2012)
14. D.C. Carter, X.-M. He, S.H. Munson, P.D. Twigg, K.M. Gernert, M.B. Broom, T.Y. Miller, Three-dimensional structure of human serum albumin. Science **244**, 1195–1198 (1989)
15. A.K. Wright, M.R. Thompson, Hydrodynamic structure of bovine serum albumin determined by transient electric birefringence. Biophys. J. **15**, 137–141 (1975)
16. X.M. He, D.C. Carter, Atomic structure and chemistry of human serum albumin. Nature **358**, 209–215 (1992)
17. C. Röcker, M. Pötzl, F. Zhang, W.J. Park, G.U. Nienhaus, A quantitative fluorescence study of protein monolayer formation on colloidal nanoparticles. Nat. Nano **4**, 577–580 (2009)
18. T.J. Su, J.R. Lu, R.K. Thomas, Z.F. Cui, J. Penfold, The conformational structure of bovine serum albumin layers adsorbed at the silica-water interface. J. Phys. Chem. B **102**, 8100–8108 (1998)
19. L.A. Girifalco, M. Hodak, R.S. Lee, Carbon nanotubes, buckyballs, ropes, and a universal graphitic potential. Phys. Rev. B **62**, 13104–13110 (2000)
20. M. Hodak, L.A. Girifalco, Fullerenes inside carbon nanotubes and multi-walled carbon nanotubes: optimum and maximum sizes. Chem. Phys. Lett. **350**, 405–411 (2001)
21. D. Baowan, B.J. Cox, J.M. Hill, Instability of C_{60} fullerene interacting with lipid bilayer. J. Mol. Model. **18**, 549–557 (2012)

22. D. Baowan, H. Peuschel, A. Kraegeloh, V. Helms, Energetics of liposomes encapsulating silica nanoparticles. J. Mol. Model. **19**, 2459–2472 (2013)
23. W.C. Still, A. Tempczyk, R.C. Hawley, T. Hendrickson, Semianalytical treatment of solvation for molecular mechanics and dynamics. J. Am. Chem. Soc. **112**, 6127–6129 (1990)
24. E.R. Cruz-Chu, A. Aksimentiev, K. Schulten, Water-silica force field for simulating nanodevices. J. Phys. Chem. B **110**, 21497–21508 (2006)
25. D. Makimura, C. Metin, T. Kabashima, T. Matsuoka, Q.P. Nguyen, C.R. Miranda, Combined modeling and experimental studies of hydroxylated silica nanoparticles. J. Mater. Sci. **45**, 5084–5088 (2010)
26. S.L. Mayo, B.D. Olafson, W.A. Goddard III, A generic force field for molecular simulations. J. Phys. Chem. **94**, 8897–8909 (1990)
27. D. Baowan, N. Thamwattana, Modelling selective separation of trypsin and lysozyme using mesoporous silica. Micro. Meso. Mater. **176**, 209–214 (2013)

RSC Advances

PAPER

Cite this: *RSC Adv.*, 2015, **5**, 5508

Instability of carbon nanoparticles interacting with lipid bilayers

Duangkamon Baowan,*[a] Barry J. Cox[b] and James M. Hill[b]

Received 30th October 2014
Accepted 10th December 2014

DOI: 10.1039/c4ra13496f

www.rsc.org/advances

As a first step in the study of the toxicity of nanoparticles, we investigate here the energy behaviour of three distinct carbon nanoparticles interacting with a lipid bilayer; namely fullerenes, nanotubes and nanocones, using the Lennard-Jones potential together with the continuous approximation. For an assumed circular hole in the lipid bilayer, a relation for the molecular interaction energy is determined, involving the circular hole radius and the perpendicular distance of the nanoparticle from the hole. For each nanoparticle, the relation between the minimum energy location and the hole radius b is found, and for example, for a fullerene of radius 15 Å, for $b > 19.03$ Å, the nanoparticle relocates from the surface of the bilayer to the interior, and as the hole radius increases further it moves to the centre of the bilayer, remaining there for increasing hole radii. When the system has no external forces, the nanoparticle will not penetrate through the lipid bilayer but rather remains enclosed between the two layers.

1 Introduction

Due to the large number of possible applications of nanoparticles in cosmetic and medical products, the possible hazards of nanoparticles in the human body are a major concern. A worst-case scenario is that nanoparticles might act as a centre of high activity and cause health issues such as skin damage or even induce diseases such as cancer. To understand the toxicity of nanoparticles, the interaction behaviour between the particles and the cell membrane is examined in order to understand the translocation of molecules into cells.

Yang and Ma[1] determine the effect of the nanoparticle size and shape on the relocation procedure across the lipid bilayer as a guide to designing the architecture of nano-cargos. They conclude that particle geometry is the key to successful nanoparticle design. The navigation of different shaped nanoparticles through biological processes is extensively reviewed by Toy *et al.*[2] Further, it has been shown that an external force is required to transport an alien particle into cells.[1,3–6] Here, we use mathematical modelling to investigate the van der Waals interaction between carbon nanostructures and a lipid bilayer. Three geometries of carbon nanostructures are considered, namely fullerenes, nanotubes and nanocones which are assumed to be the foreign particle penetrating through the dipalmitoylphosphatidylcholine (DPPC) lipid.

During the past two decades, various atomistic molecular mechanics force fields have been parameterized enabling the dynamic simulation of lipid bilayers.[7–9] Recently, several coarse grained models have been used for lipid membranes[10–14] to deal with the large dimensions of membrane compartments. Marrink *et al.*[11] describe the parametrization of a coarse grained model for a DPPC lipid system. Furthermore, Shelley *et al.*[12] use a coarse grained model to study the structure and self-assembly of phospholipids bilayers. Another coarse-grained force field for zwitterionic lipids and based on fitted thermodynamic and structural properties has been developed by Shinoda *et al.*[14] Besides force field descriptions for the energy of molecular conformations that use either atomistic or coarse grained descriptions, such systems can also be studied using a continuous approach. In the continuous approximation, one assumes that discrete atomic arrangements can be replaced by a uniform atomic distribution, so that the total interaction energy between two molecules can be evaluated using an integral technique. The continuous approach has been successfully applied by a number of authors to determine the molecular interaction energy of nanostructures.[15–20]

The instability of C_{60} fullerene interaction with DPPC lipid bilayer has been studied by the present authors[19] utilizing the Lennard-Jones potential function and the continuous approximation, and the relocation of the fullerene from the surface to the interior of the lipid has been reported. Further, Baowan *et al.*[20] use the same technique to determine the interaction energy of silica nanoparticle encapsulated inside a liposome, spherical lipid bilayer. Both van der Waals and electrostatic interactions are taken into account but in terms of the stability of the system the van der Waals energy plays the important role.

In this paper, we follow[19,20] and use the Lennard-Jones potential function together with the continuous approximation to determine the molecular interaction energy between

[a]*Department of Mathematics, Faculty of Science, Mahidol University, Rama VI, Bangkok 10400, Thailand. E-mail: duangkamon.bao@mahidol.ac.th; Fax: +66 2 201 5343; Tel: +66 2 201 5340*

[b]*Nanomechanics Group, School of Mathematical Sciences, The University of Adelaide, South Australia 5005, Australia*

This journal is © The Royal Society of Chemistry 2015

certain carbon nanostructures and a DPPC lipid bilayer. Using different particle geometries, we investigate the penetration behaviour of the particles through an assumed circular hole in the lipid bilayer. The model formulations for the lipid bilayer and the carbon nanoparticles are detailed in the following section. In Section 3, the mathematical derivations for the three particle geometries interacting with the lipid are presented. Further, numerical results are given in Section 4, and finally, a brief summary of the work is presented in Section 5.

2 Model

This study aims at computing the energy of systems comprising carbon nanoparticles and a lipid bilayer which is assumed to be large enough to represent a cell membrane. The penetration behaviour of the nanoparticles through an assumed circular hole of radius b in the bilayer is determined. Three distinct shapes of the nanoparticles are assumed as possible structures of alien particles penetrating through the lipid bilayer, which are fullerenes, nanotubes and nanocones, and these are modelled as spheres, cylinders and cones, respectively. For the nanotubes and nanocones, two distinct configurations are considered (see Fig. 1). The carbon nanotubes are assumed to be both short and thin cylinders, and the nanocones are assumed to be one of vertical down and that of vertical up, as shown in Fig. 1(b–e). In order to make an energy comparison, we assume that all the nanoparticles are carbon nanostructures and all carbon atoms are uniformly distributed over the surfaces of the molecules with the same atomic surface densities $\eta_c = 0.3812$ Å^{-2}. Further, the particles are assumed to be located on the z-axis a distance Z above the hole in the lipid bilayer where Z is measured from the centres of the sphere and the cylinder and it is taken to be the closest position of the cone to the bilayer as indicated in Fig. 1.

Here, only the van der Waals interaction arising from the Lennard-Jones function is taken into account, since it has been shown that the electrostatic energy plays only a minor effect on the systems.[20] The 6–12 Lennard-Jones function is given by

$$\Phi = -\frac{A}{\rho^6} + \frac{B}{\rho^{12}} = 4\varepsilon\left[-\left(\frac{\sigma}{\rho}\right)^6 + \left(\frac{\sigma}{\rho}\right)^{12}\right], \quad (1)$$

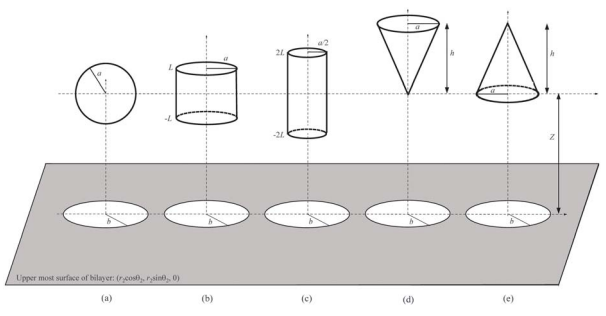

Fig. 1 Three shapes with five possible configurations of carbon nanoparticles located a distance Z above lipid bilayer.

where ρ denotes the distance between two typical points, and A and B are attractive and repulsive Lennard-Jones constants, respectively. Further, ε denotes the well depth and σ is the van der Waals diameter, and from which we may deduce $A = 4\varepsilon\sigma^6$ and $B = 4\varepsilon\sigma^{12}$.

The continuous approach assumes that the atoms at discrete locations on the molecule are averaged over a surface or a volume and the molecular interatomic energy is obtained by integrating over the surface or the volume of each molecule, given by

$$E = \eta_1\eta_2\int_{S_1}\int_{S_2}\left(-\frac{A}{\rho^6} + \frac{B}{\rho^{12}}\right)\mathrm{d}S_2\,\mathrm{d}S_1,$$

where η_1 and η_2 represent the mean surface densities or the mean volume densities of atoms on each molecule. For convenience, we may define the integral I_n as

$$I_n = \int_{S_1}\int_{S_2}\rho^{-2n}\,\mathrm{d}S_2\,\mathrm{d}S_1, \quad n = 3,\ 6, \quad (2)$$

so that, $E = \eta_1\eta_2(-AI_3 + BI_6)$.

The Lennard-Jones potential function together with the continuous approach has been successfully applied by a number of authors to determine the molecular interaction energy of nanostructures, see for example Girifalco *et al.*,[15] Hodak and Girifalco,[16] Cox *et al.*,[17,18] and Baowan *et al.*[19,20] In the first two studies,[15,16] analytical expressions are derived for the potential energies for various arrangements of a carbon nanotube and a C_{60} fullerene. Cox *et al.*[17,18] use elementary mechanical principles together with the continuous approach to study the oscillatory behavior of a C_{60} fullerene inside carbon nanotubes of various sizes. The structural behaviour and oscillatory frequency obtained there are in good agreement with molecular dynamics simulations of Qian *et al.*[21] and Liu *et al.*[22]

Here, dipalmitoylphosphatidylcholine (DPPC) is adopted as the lipid model which is represented in the MARTINI force field by a head group, consisting of choline (Q_0) and phosphate (Q_a) groups, an intermediate layer of a glycerol group (N_a) and a carbon tail group (C_1).[11] In this paper, the spacing between the two layers of lipids is assumed to be 3.36 Å.[19] The positions for choline, phosphate and glycerol groups are taken from the work of Petrache *et al.*,[23] and they are detailed in Fig. 2(b) where the upper head group H_1 is assumed to be located on the xy-plane, $z_2 = 0$, and the other five positions of the five lipid bilayer layers are measured in a negative direction of z_2-axis. The Lennard-Jones constants for the lipid bilayer are taken from the work of Marrink *et al.*,[11] where the carbon nanoparticles are assumed to be an apolar group of type C_1. The numerical values of the Lennard-Jones constants used in this model are given in Table 1.

The coarse grained model assigns two interaction sites to the head group, one for the choline group and one for the phosphate group; two interaction sites to the intermediate layer; and eight interaction sites to the tail group.[11] We assume that the intermediate group of the bilayer can be represented as a flat plane, so that the mean atomic surface density for the intermediate group, η_{inter}, is given by 2/65 Å^{-2}. Here, the factor 2 reflects the two interaction sites for the intermediate layer in the MARTINI force field. Also the tail group is approximated as a

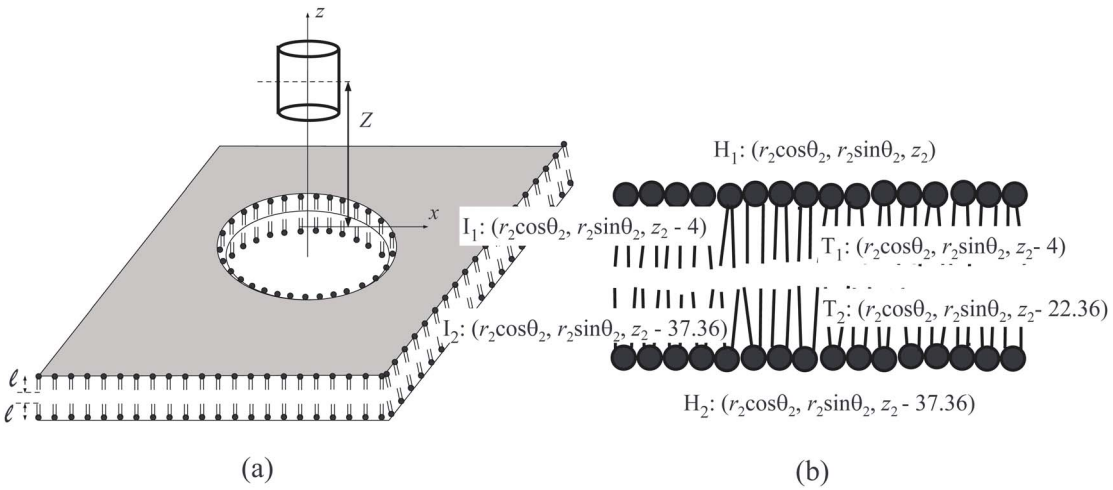

Fig. 2 Model for (a) a hole in bilayer and (b) structural dimensions of lipid bilayer where H_1 and H_2 represent upper and lower head groups, I_1 and I_2 denote upper and lower intermediate layers and T_1 and T_2 are upper and lower tail groups.

Table 1 Numerical values of Lennard-Jones constants for DPPC lipid interacting with apolar carbon nanostructures of type C_1[11]

Interaction	ε (eV)	σ (Å)	A (eV × Å^6)	B (eV × Å^{12})
Head group	2.073×10^{-2}	6.2	4.709×10^3	2.675×10^8
Intermediate layer	2.798×10^{-2}	4.7	1.207×10^3	1.301×10^7
Tail group	3.627×10^{-2}	4.7	1.564×10^3	1.686×10^7

box with a thickness of a tail length $\ell = 15$ Å, and the mean atomic volume density for the tail group, η_{tail}, is given by $8/(65\ell)$ Å^{-3}. Again, the factor 8 reflects the eight interaction sites of the tail group. Similarly, the head group can be modelled as an infinite box of thickness of 4 Å. Consequently, the mean atomic volume density of the head group is $\eta_{\text{head}} = 1/(130)$ Å^{-3}. We note that the value 65 Å^2 represents a lipid head group area.

3 Mathematical derivation

In this study, surface and volume integration techniques are applied to evaluate the total interaction energy between a lipid bilayer and a carbon nanostructure, and the total energy of each system is assumed to comprise:

1. Interactions between the surface of a nanoparticle and the volumes of upper and lower lipid head groups at distances Z and Z + 37.36 Å, respectively.

2. Interactions between the surface of a nanoparticle and the surfaces of upper and lower lipid intermediate layers at distances Z + 4 and Z + 37.36 Å, respectively.

3. Interactions between the surface of a nanoparticle and the volumes of upper and lower lipid tail groups at distances Z + 4 and Z + 22.36 Å, respectively.

In order to make energetic comparisons, the surface areas of the carbon nanoparticles considered here are assumed to be equal, and their mathematical derivations are detailed in the following subsections.

3.1 Spherical nanoparticle

A sphere of radius a is considered with centre assumed to be located at a distance Z measured from the uppermost surface of the lipid bilayer as shown in Fig. 1(a). Further, the lipid bilayer is assumed to have a circular hole of radius $b > a$. The mathematical details for the interaction energy between a sphere and a flat plane, and that between a sphere and a box can be found in,[19] and for the completeness the results are restated here. We comment that in the previous work,[19] the head group of the bilayer is assumed to be a flat plane whereas the tail group is represented by a box of thickness ℓ and with no intermediate layer. In order to capture all energy contributions, an improved model of the lipid bilayer is presented here such that the effect of the intermediate layer is included and the additional atoms in the head group are combined.

The interaction energy between the sphere and the flat plane or the box may be shown (see ref. 19) to be given by

$$E_{\text{sphere}} = \pi\eta_c\eta^*\Big[-4aA\left(J_3 + 2a^2J_4\right) + \frac{4aB}{5}\left(5J_6 + 80a^2J_7 + 336a^4J_8 + 512a^6J_9 + 256a^8J_{10}\right)\Big], \quad (3)$$

where η^* is a mean surface or a mean volume density of the lipid bilayer. In the case of the intermediate layer, we have

$$J_n^{\text{p}} = \frac{\pi}{(n-1)}\frac{1}{(Z^2 + b^2 - a^2)^{n-1}},$$

where the superscript p refers to the flat plane interaction. For the head and the tail groups of thickness ℓ, we may deduce

$$J_n^{\text{b}} = \frac{\pi}{(n-1)(b^2-a^2)^{n-2}}\int_{\tan^{-1}\left(\frac{Z}{\sqrt{b^2-a^2}}\right)}^{\tan^{-1}\left(\frac{Z+\ell}{\sqrt{b^2-a^2}}\right)}\cos^{2n-4}\phi\,\mathrm{d}\phi,$$

where the superscript b represents the box interaction, and the above integral can be found in ref. 24 (p. 153, no. 2.513.3), from which we may deduce

 This journal is © The Royal Society of Chemistry 2015

$$\int \cos^{2m}\phi \, \mathrm{d}\phi = \frac{1}{2^{2m}}\left[\binom{2m}{m}\phi + \sum_{k=0}^{m-1}\binom{2m}{k}\frac{\sin[2(m-k)\phi]}{m-k}\right], \quad (4)$$

where $\binom{x}{y}$ is the usual binomial coefficients and $m = n - 2$. We note that the thickness of the head group is taken to be $\ell = 4$ Å, and that of the tail group is $\ell = 15$ Å.

3.2 Cylindrical nanoparticle

The cylindrical carbon nanostructure, or carbon nanotube, of radius a and half-length L is assumed to be located co-axially on the z-axis with its centre being a distance Z above the lipid bilayer as shown in Fig. 1(b). A typical surface element of the cylinder has coordinates given by $(a\cos\theta_1,\ a\sin\theta_1,\ z_1 + Z)$ where $0 < \theta_1 < 2\pi$ and $-L < z_1 < L$.

Firstly, we determine the interaction energy between a flat plane for which a typical surface element has coordinates $(r\cos\theta_2,\ r\sin\theta_2,\ 0)$ where $b < r < \infty$, $0 < \theta_2 < 2\pi$ and $b > a$ denotes the hole radius in the bilayer. The distance of the flat plane to the surface of the cylinder is given by

$$\begin{aligned}\rho^2 &= (a\cos\theta_1 - r\cos\theta_2)^2 + (a\sin\theta_1 - r\sin\theta_2)^2 + (z_1 + Z)^2\\ &= (a-r)^2 + (z_1+Z)^2 + 4ar\sin^2[(\theta_1-\theta_2)/2],\end{aligned}$$

and the integral I_n defined by (2) may be written as

$$I_n^{\mathrm{p}} = \int_0^{2\pi}\int_b^{\infty}\int_0^{2\pi}\int_{-L}^{L} ar \times \frac{\mathrm{d}z_1\,\mathrm{d}\theta_1\,\mathrm{d}r\,\mathrm{d}\theta_2}{\left\{(a-r)^2 + (z_1+Z)^2 + 4ar\sin^2[(\theta_1-\theta_2)/2]\right\}^n}, \quad (5)$$

where $F(a, b; c, z)$ is the usual hypergeometric function. Further, we may use a Pfaff transformation[24] to truncate the infinite series summation of the hypergeometric function, so that K_n becomes

$$\begin{aligned}K_n &= \frac{4\pi^2}{\alpha^n}\left(\frac{\alpha}{\alpha+\beta}\right)^{1/2} F\left(1-n,\ \frac{1}{2};\ 1;\ \frac{\beta}{\alpha+\beta}\right)\\ &= \frac{4\pi^2}{\alpha^{n-1/2}(\alpha+\beta)^{1/2}}\sum_{k=0}^{n-1}\frac{(1-n)_k(1/2)_k}{(k!)^2}\left(\frac{\beta}{\alpha+\beta}\right)^k.\end{aligned}$$

Consequently, there are two remaining integrals for I_n^{p}

$$I_n^{\mathrm{p}} = 4\pi^2 a\sum_{k=0}^{n-1}\frac{(1-n)_k(1/2)_k}{(k!)^2}(4a)^k \times \int_b^{\infty}\int_{-L}^{L}\frac{r^{k+1}\,\mathrm{d}z_1\,\mathrm{d}r}{\left[(a-r)^2+(z_1+Z)^2\right]^{n-1/2}\left[(a+r)^2+(z_1+Z)^2\right]^{k+1/2}}. \quad (7)$$

The above integral may be performed numerically utilizing the algebraic package MAPLE, and the total interaction energy between the cylinder of length $2L$ and the intermediate layer of the lipid is given by

$$E_{\mathrm{cylinder}}^{\mathrm{p}} = \eta_{\mathrm{c}}\eta_{\mathrm{inter}}(-AI_3^{\mathrm{p}} + BI_6^{\mathrm{p}}), \quad (8)$$

where I_n^{p} is given by (7).

In terms of the interaction energy between a cylinder and a box of thickness ℓ, a similar procedure is undertaken with the term $(z_1 + Z)$ replaced by $(z_1 + Z - z_2)$ and $-\ell < z_2 < 0$, and the integral I_n defined by (2) becomes

$$I_n^{\mathrm{b}} = 4\pi^2 a\sum_{k=0}^{n-1}\frac{(1-n)_k(1/2)_k}{(k!)^2}(4a)^k\int_{-\ell}^{0}\int_b^{\infty}\int_{-L}^{L}\frac{r^{k+1}\,\mathrm{d}z_1\,\mathrm{d}r\,\mathrm{d}z_2}{\left[(a-r)^2+(z_1+Z-z_2)^2\right]^{n-\frac{1}{2}}\left[(a+r)^2+(z_1+Z-z_2)^2\right]^{k+\frac{1}{2}}}, \quad (9)$$

and again the superscript p refers to the plane interaction. We now define

$$K_n = \int_0^{2\pi}\int_0^{2\pi}\frac{1}{\{\alpha+\beta\sin^2[(\theta_1-\theta_2)/2]\}^n}\,\mathrm{d}\theta_1\,\mathrm{d}\theta_2, \quad (6)$$

where $\alpha = (a-r)^2 + (z_1+Z)^2$ and $\beta = 4ar$. It can be shown that K_n is independent of either θ_1 or θ_2,[25] and we have simply

$$K_n = 8\pi\int_0^{\pi/2}\frac{1}{(\alpha+\beta\sin^2 x)^n}\,\mathrm{d}x.$$

On letting $u = \sin^2 x$, we may deduce

$$\begin{aligned}K_n &= \frac{4\pi}{\alpha^n}\int_0^1 u^{-1/2}(1-u)^{-1/2}\left(1+\frac{\beta}{\alpha}u\right)^{-n}\mathrm{d}u\\ &= \frac{4\pi^2}{\alpha^n}F\left(n,\ \frac{1}{2};\ 1;\ -\frac{\beta}{\alpha}\right),\end{aligned}$$

where the superscript b denotes the box interaction. Again, we have $\ell = 4$ Å for the thickness of the lipid bilayer head group and $\ell = 15$ Å for that of the tail group. The distance in the z-direction for each layer of the lipid is detailed in Fig. 2(b), and the total interaction energy between the cylinder of length $2L$ and the head or the tail group of the lipid bilayer is

$$E_{\mathrm{cylinder}}^{\mathrm{b}} = \eta_{\mathrm{c}}\eta^*(-AI_3^{\mathrm{b}} + BI_6^{\mathrm{b}}), \quad (10)$$

where η^* can be either η_{head} or η_{tail}, and I_n^{b} is given by (9).

3.3 Conical nanoparticle

In this subsection, we consider both a "vertically down" cone and a "vertically up" cone for which mathematical determinations are similar except for the limits of integration in the z-direction.

Firstly, we consider the vertically down cone as shown in Fig. 1(d). A typical point on the cone has coordinates $(r_1\cos\theta_1,$

$r_1 \sin\theta_1, z_1 + Z$) where $r_1 = az_1/h$ and $0 < z_1 < h$. Here, Z is the distance from the upper lipid bilayer surface to the cone vertex, a is the cone base radius and h is the cone height. As with the cylindrical nanoparticle, the coordinates for the flat plane are ($r_2 \cos\theta_2$, $r_2 \sin\theta_2$, 0) where $b < r_2 < \infty$ and $0 < \theta_2 < 2\pi$, so that the distance between the flat plane and the surface of the cone is given by

$$\rho^2 = [(a/h)z_1 - r_2]^2 + (z_1 + Z)^2 + 4(a/h)z_1 r_2 \sin^2[(\theta_1 - \theta_2)/2].$$

The integral I_n defined by (2) becomes

$$I_n^{\mathrm{p}} = \frac{\tan(\phi/2)}{\cos(\phi/2)} \int_0^{2\pi}\int_b^{\infty}\int_0^{2\pi}\int_0^{h} \frac{z_1 r_2 \,\mathrm{d}z_1\,\mathrm{d}\theta_1\,\mathrm{d}r_2\,\mathrm{d}\theta_2}{\left\{\left[\left(\frac{a}{h}\right)z_1 - r_2\right]^2 + (z_1+Z)^2 + 4\left(\frac{a}{h}\right)z_1 r_2 \sin^2\left(\frac{\theta_1-\theta_2}{2}\right)\right\}^{n}}, \tag{11}$$

where ϕ is a cone angle, $\tan(\phi/2) = a/h$, $\cos(\phi/2) = h/\sqrt{a^2+h^2}$ and p indicates the plane interaction. We then write the above integral in terms of K_n defined by (6), and carry out precisely the same derivation as described in Section 3.2 but in this case we have $\alpha = [(a/h)z_1 - r_2]^2 + (z_1 + Z)^2$ and $\beta = 4(a/h)z_1 r_2$, and I_n^{p} for the vertically down cone becomes

$$I_n^{\mathrm{p}} = 4\pi^2 \frac{\tan(\phi/2)}{\cos(\phi/2)} \sum_{k=0}^{n-1} \frac{(1-n)_k (1/2)_k}{(k!)^2} \left(\frac{4a}{h}\right)^k \int_b^{\infty}\int_0^{h} \frac{(z_1 r_2)^{k+1}\mathrm{d}z_1\,\mathrm{d}r_2}{\left\{\left[\left(\frac{a}{h}\right)z_1 - r_2\right]^2 + (z_1+Z)^2\right\}^{n-\frac{1}{2}} \left\{\left[\left(\frac{a}{h}\right)z_1 + r_2\right]^2 + (z_1+Z)^2\right\}^{k+\frac{1}{2}}}. \tag{12}$$

The interaction energy between the vertically down cone and the intermediate layer is given by

$$E_{\mathrm{cone}}^{\mathrm{p}} = \eta_{\mathrm{c}}\eta_{\mathrm{inter}}(-AI_5^{\mathrm{p}} + BI_6^{\mathrm{p}}), \tag{13}$$

where in this case I_n^{p} is defined by (12).

For the interaction energy between a box of thickness ℓ and a cone, there is an extra integral with respect to z_2 that must be determined. The term $(z_1 + Z)$ is replaced by $(z_1 + Z - z_2)$ where $-\ell < z_2 < 0$, and we may deduce

$$I_n^{\mathrm{b}} = 4\pi^2 \frac{\tan(\phi/2)}{\cos(\phi/2)} \sum_{k=0}^{n-1} \frac{(1-n)_k (1/2)_k}{(k!)^2} \left(\frac{4a}{h}\right)^k \int_{-\ell}^{0}\int_b^{\infty}\int_0^{h} \frac{(z_1 r_2)^{k+1}\mathrm{d}z_1\,\mathrm{d}r_2\,\mathrm{d}z_2}{\left\{\left[\left(\frac{a}{h}\right)z_1 - r_2\right]^2 + (z_1+Z-z_2)^2\right\}^{n-\frac{1}{2}} \left\{\left[\left(\frac{a}{h}\right)z_1 + r_2\right]^2 + (z_1+Z-z_2)^2\right\}^{k+\frac{1}{2}}}, \tag{14}$$

where b denotes the box interaction. Then the total interaction energy between the vertically down cone and the head or the tail group can be written as

$$E_{\mathrm{cone}}^{\mathrm{b}} = \eta_{\mathrm{c}}\eta^*(-AI_3^{\mathrm{b}} + BI_6^{\mathrm{b}}), \tag{15}$$

where η^* can be either η_{head} or η_{tail} and I_n^{b} is given by (14).

For the vertically up cone, both the interaction between the cone and the flat plane and that between the cone and the box can be determined in precisely the same manner as that described for the vertically down cone. However, for the vertically up cone the integration with respect to z_1 appearing in (12) and (14) is evaluated from 0 to $-h$.

4 Numerical results

Interaction energies for the three carbon nanoparticle geometries involving five configurations and the lipid bilayer are determined. In an attempt to make meaningful comparison, we assume that the surface areas of the particles are all equal, and we fix the spherical radius, short cylindrical radius and two cone base radii to be a. Moreover, the radius of the thin cylinder is assumed to be $a/2$ to represent a long thin carbon nanotube. As a result, the length of the short cylinder becomes $L = a$, the heights of the two cones are $h = a\sqrt{15}$, and the length of the thin cylinder is $L = 2a$.

Firstly, we determine the equilibrium positions for the five carbon nanostructures of $a = 15$ Å assumed to be interacting with a perfect lipid bilayer without any hole. The energy profiles are graphically shown in Fig. 3 where the distance δ is referred to the closest distance from the upper lipid head group to the

This journal is © The Royal Society of Chemistry 2015

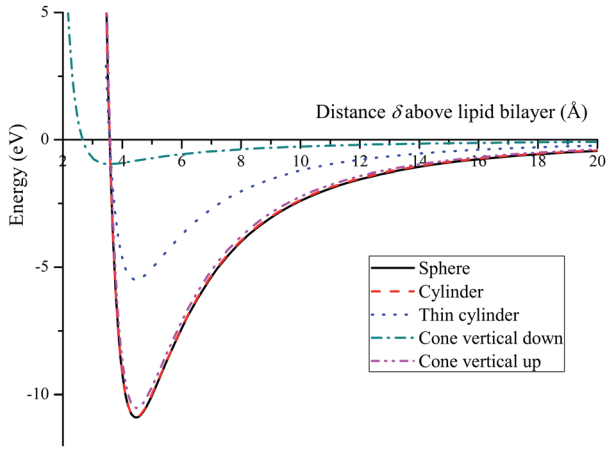

Fig. 3 Energy profiles for five configurations of carbon nanoparticles of $a = 15$ Å interacting with lipid bilayer without hole where δ refers to the closest distance from the upper lipid head group to the particles and $\delta = Z - a$ for sphere and short cylinder, $\delta = Z - 2a$ for thin cylinder, and $\delta = Z$ for cones.

particles. This is $\delta = Z - a$ for the cases of the sphere and the short cylinder, $\delta = Z - 2a$ for the thin cylinder, and $\delta = Z$ for the cones. It can be seen that the sphere and the cylinder of the same radii have the same behaviour in terms of the energy values and the equilibrium spacings δ. The cone of vertical up also has a similar manner. This is because a number of carbon atoms near the lipid bilayer for these three cases are equivalent and the equilibrium distances δ are approximately 4.45 Å above the bilayer. A number of carbon atoms around the tube end of the thin cylinder of radius $a/2$ is a half of the short cylinder, so that its energy value reduces by a half but the equilibrium spacing still be 4.45 Å. In the case of the vertically down cone, there are only a few carbon atoms at the vertex giving rise to a low interaction energy. However, this makes the cone move closer to the bilayer with an equilibrium spacing of 3.58 Å. We comment that the same energy profiles for larger carbon nanoparticles are observed, and that they differ only in the magnitude of the energy.

Next, we study the relation between the distance Z and the hole in the lipid bilayer of radius b at the equilibrium positions of the particles. A positive value of Z indicates that the particle is located above the bilayer and a negative value of Z indicates that the particle has penetrated through the bilayer. Two sizes of the carbon nanoparticles which are $a = 15$ and 50 Å are determined to demonstrate the different penetration behaviours between particles smaller than the bilayer thickness and larger than the bilayer thickness, respectively. We note that in this study the thickness of the lipid bilayer is taken to be 41.36 Å.

Fig. 4 shows the relation between distance Z and hole radius b for five configurations of small carbon nanostructures where surface areas are all assumed to be $4\pi a^2$ and $a = 15$ Å. The spherical particle moves closer to the bilayer as the hole radius gets larger. Once the hole radius is larger than the critical radius $b_0 > 19.03$ Å, the particle jumps into the bilayer and there are two equilibrium positions near the two head groups due to the symmetry of the two layers of lipid. Moreover, the sphere remains at the midplane of the bilayer when the hole radius is grater than 32 Å. The relocation behaviour is also observed for the two cylindrical particles with the critical hole radii b_0 of 18.15 and 11.23 Å for the short and the thin cylinders, respectively, which are around 4 Å larger than their radii. Once inside the bilayer, they will remain at the midplane. Even though the two cylinders have the similar behaviour, there are some advantages of a long thin cylinder over a short one. There will be some parts of the long thin tube passing to the other side of the bilayer which might be used for drug or gene transmission into the cell. Further, a smaller tube cross-section requires a smaller hole in the bilayer which in turn makes less disorder of lipid molecules arrangement in the cell membrane.

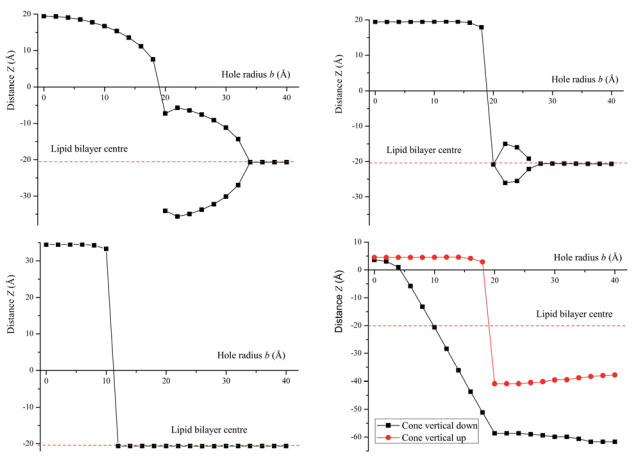

Fig. 4 Relation between distance Z and hole radius b for five small carbon nanostructures with equivalent surface area for (upper left) sphere of $a = 15$ Å, (upper right) cylinder of $a = L = 15$ Å, (lower left) thin cylinder of $2a = L/2 = 15$ Å, and (lower right) cones vertical down and vertical up of $a = 15$ and $h = 15\sqrt{15}$ Å.

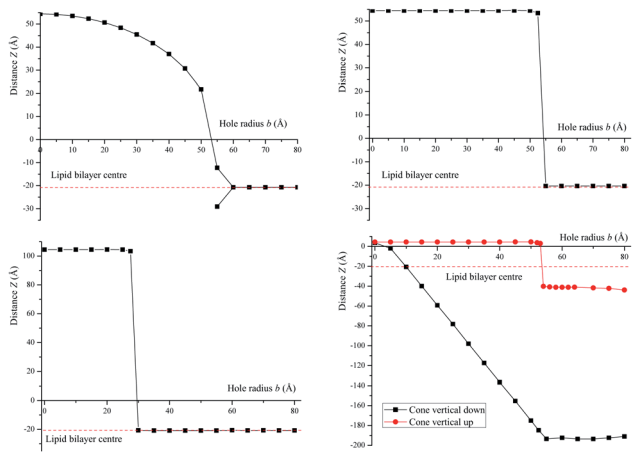

Fig. 5 Relation between distance Z and hole radius b for five small carbon nanostructures with equivalent surface area for (upper left) sphere of $a = 50$ Å, (upper right) cylinder of $a = L = 50$ Å, (lower left) thin cylinder of $2a = L/2 = 50$ Å, and (lower right) cones vertical down and vertical up of $a = 50$ and $h = 50\sqrt{15}$ Å.

The vertically up cone behaves like the cylindrical carbon nanotube, where the critical hole radius of the cone is obtained as $b_0 = 18.13$ Å. However, some parts of the cone will be on the other side of the bilayer, and may be used as a conduit to transmit other molecules into the cell. Finally, for the case of the of vertically down cone, it gradually penetrates inside the bilayer as the hole radius in the bilayer increases since the circular cone radius itself increases as it movies down. The equilibrium positions for all five configurations are all at the midplane of the two layers of lipid once the hole radius is large enough, and the penetration of the nanoparticles across the bilayer is always facilitated by an external force which is in agreement with.[1,3–6]

A similar penetration behaviour is observed for the large carbon nanoparticles of $a = 50$ Å as shown in Fig. 5. However, double minima is only occurred for the case of a spherical molecule. We also observe that the jump behaviour occurs for the sphere, two cylinders and the vertically up cone, whereas the vertically down cone gradually penetrates through the bilayer, and the external forces are required to drive the alien particles into cells.[1,3–6]

Table 2 Penetration behaviour for three geometries of five configurations of carbon nanostructures through lipid bilayer

Shapes	Penetration behaviour	Minima	b_0 (Å)
$\boldsymbol{a = 15}$ **Å**			
Sphere	Gradually jump	Double minima	19.03
Short cylinder	Jump	Double minima	18.15
Thin cylinder	Jump	One minimum	11.23
Cone of vertical down	Gradually penetrate	One minimum	—
Cone of vertical up	Jump	One minimum	18.13
$\boldsymbol{a = 50}$ **Å**			
Sphere	Gradually jump	Double minima	53.21
Short cylinder	Jump	One minimum	54.31
Thin cylinder	Jump	One minimum	29.59
Cone of vertical down	Gradually penetrate	One minimum	—
Cone of vertical up	Jump	One minimum	53.09

5 Summary

This paper presents an energetic comparison for the penetration of carbon nanostructures into a lipid bilayer. For this, the van der Waals energy is evaluated using the Lennard-Jones function and the continuous approach, which assumes that atoms in a molecule are uniformly distributed over a surface or throughout the volume of the molecule, so that an integration approach can be applied to evaluate the total energy of the system. We consider three geometries involving five distinct configurations of the nanoparticles which are a sphere, two cylinders and two cones, and we assume that all carbon atoms are distributed over their surfaces. Further, the lipid bilayer studied here is assumed to be a DPPC with two head groups, two intermediate layers and two tail groups. For this we derive analytical expressions to describe how the various energies depend on particle geometries, particle size, distance of the particle from the bilayer, and the hole size in the bilayer.

The spacing δ between the upper head group and the five particles is determined in the absence of the hole in the lipid. We find that the equilibrium location of the vertically down cone is closest to the bilayer, because of fewer carbon atoms at the vertex, inducing only a weak repulsion energy. The other four configurations have comparable values of the spacings δ. However, the energy for the thin carbon nanotube is one half of the energies of the sphere, short cylinder and vertically up cone since the number of atoms at the tube end is approximately one half of the other three shapes.

Our study shows that the particles locate inside the bilayer when the hole in the bilayer is large enough, around 4 Å greater that the particle's radius. However, they are more likely to remain between the two layers of the lipid and do not move across to be inside the cell. Therefore, external forces are required for the penetration of the nanoparticles through the cell. The penetration behaviour and the critical hole radius b_0 for the carbon nanoparticles are summarized in Table 2.

Nanocapsules for drug and gene delivery might be designed from these five simple structures. The spherical and the vertically down cone capsules may be utilized for chemical reactions at the surface of the cell membrane. This is because we may choose the size of the capsule for a specific lipid bilayer hole, and the capsule will stick at the upper layer of the lipid and does not move inside the cell membrane. However, if the adsorption energy is too low, it might not be a good candidate for the surface chemical reaction since the interaction between membrane and nanoparticle might be too weak. The cylindrical and vertically up cone capsules may escape a fast reaction at the surface of the cell membrane because a jump behaviour occurs for a specific lipid hole size. Further, for a tube with length longer than the thickness of the bilayer, there will be some parts of the tube getting to the other side of the cell membrane which may be used to transport the drug or the gene into cells. Using general analytical expressions for the total molecular energy of the system, our work can be viewed as a first step toward the study of transportation of nanoparticles through or inside cells.

Acknowledgements

DB gratefully thanks the Endeavour Research Scheme for the provision of an Endeavour Postdoctoral Fellowship. Financial support from the Thailand Research Fund (TRG5680072) is acknowledged.

References

1 K. Yang and Y. Q. Ma, *Nat. Nanotechnol.*, 2010, **5**, 579–583.
2 R. Toy, P. M. Peiris, K. B. Ghaghada and E. Karathanasis, *Nanomedicine*, 2014, **9**, 121–134.
3 I. Obataya, C. Nakamura, S. Han, N. Nakamura and J. Miyake, *Nano Lett.*, 2005, **5**, 27–30.
4 X. Chen, A. Kis, A. Zettle and C. R. Bertozzi, *Proc. Natl. Acad. Sci. U. S. A.*, 2007, **104**, 8218–8222.
5 I. U. Vakarelski, S. C. Brown, K. Higashitani and B. M. Moudgil, *Langmuir*, 2007, **23**, 10893–10896.

 This journal is © The Royal Society of Chemistry 2015

6 S. Hong, *et al.*, *Bioconjugate Chem.*, 2006, **17**, 728–734.
7 W. L. Ash, M. R. Zlomislic, E. O. Oloo and D. P. Tieleman, *Biochim. Biophys. Acta*, 2004, **1666**, 158–189.
8 M. L. Berkowitz, D. L. Bostick and S. Pandit, *Chem. Rev.*, 2006, **106**, 1527–1539.
9 S. W. I. Siu, R. Vácha, P. Jungwirth and R. A. Böckmann, *J. Chem. Phys.*, 2008, **128**, 125103.
10 J. Wong-Ekkabut, S. Baoukina, W. Triampo, I. M. Tang, D. P. Tieleman and L. Monticelli, *Nat. Nanotechnol.*, 2008, **3**, 363–368.
11 S. J. Marrink, H. J. Risselada, S. Yefimov, D. P. Tieleman and A. H. de Vries, *J. Phys. Chem. B*, 2007, **111**, 7812–7824.
12 J. C. Shelley, M. Y. Shelley, R. C. Reeder, S. Bandyopadhyay, P. B. Moore and M. L. Klein, *J. Phys. Chem. B*, 2001, **105**, 9785–9792.
13 E. J. Wallace and M. S. P. Sansom, *Nano Lett.*, 2007, **7**, 1923–1928.
14 W. Shinoda, R. DeVane and M. L. Klein, *J. Phys. Chem. B*, 2010, **114**, 6836–6849.
15 L. A. Girifalco, M. Hodak and R. S. Lee, *Phys. Rev. B: Condens. Matter Mater. Phys.*, 2000, **62**, 13104–13110.
16 M. Hodak and L. A. Girifalco, *Chem. Phys. Lett.*, 2001, **350**, 405–411.
17 B. J. Cox, N. Thamwattana and J. M. Hill, *Proc. R. Soc. A*, 2007, **463**, 461–476.
18 B. J. Cox, N. Thamwattana and J. M. Hill, *Proc. R. Soc. A*, 2007, **463**, 477–494.
19 D. Baowan, B. J. Cox and J. M. Hill, *J. Mol. Model.*, 2014, **18**, 549–557.
20 D. Baowan, H. Peuschel, A. Kraegeloh and V. Helms, *J. Mol. Model.*, 2013, **19**, 2459–2472.
21 D. Qian, W. K. Liu and R. S. Ruoff, *J. Phys. Chem. B*, 2001, **105**, 10753–10758.
22 P. Liu, Y. W. Zhang and C. Lu, *J. Appl. Phys.*, 2005, **97**, 094313.
23 H. I. Petrache, S. E. Feller and J. F. Nagle, *Biophys. J.*, 1997, **70**, 2237–2242.
24 I. S. Gradshteyn and I. M. Ryzhik, *Table of Integrals, Series, and Products*, Academic Press, 7th edn, 2007.
25 D. Baowan, N. Thamwattana and J. M. Hill, *Comm Nonlinear Sci Numer Simulat*, 2008, **13**, 1431–1447.

This journal is © The Royal Society of Chemistry 2015